Article

Cell Reports

Discovery and Characterization of an Endogenous CXCR4 Antagonist

Graphical Abstract

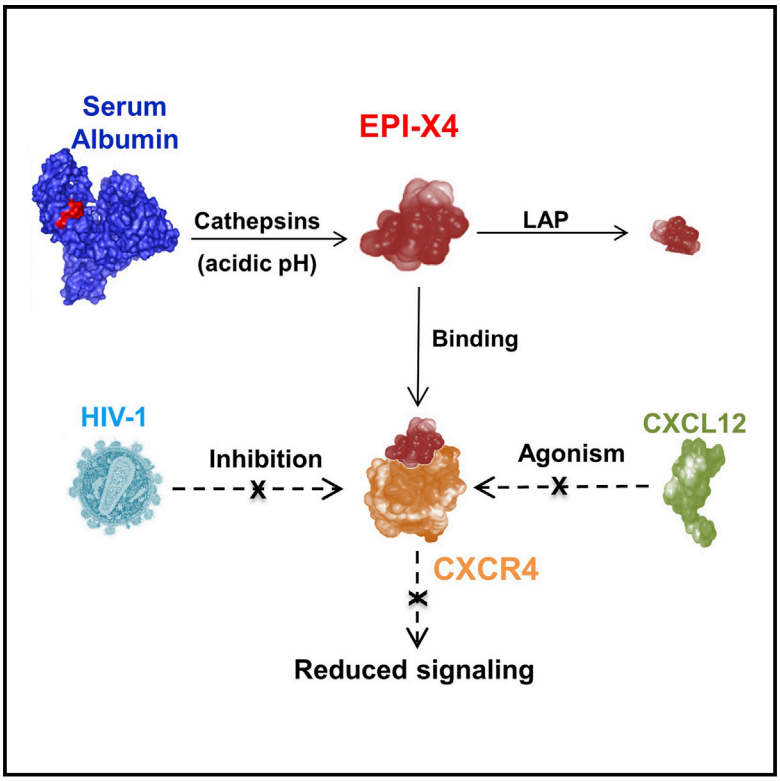

Authors

Onofrio Zirafi, Kyeong-Ae Kim, ..., Frank Kirchhoff, Jan Münch

Correspondence

jan.muench@uni-ulm.de

In Brief

The CXCL12-CXCR4 axis is involved in many physiological processes. Zirafi et al. show that an endogenous fragment of human serum albumin (LVRYTKKVPQVSTPTL) efficiently suppresses CXCR4 signaling and inhibits infection by CXCR4-tropic HIV-1 strains.

Highlights

- The albumin fragment EPI-X4 is a highly specific endogenous CXCR4 antagonist
- EPI-X4 blocks CXCL12-mediated CXCR4 signaling and cellular migration
- EPI-X4 mobilizes hematopoietic cells and inhibits inflammatory responses in vivo
- EPI-X4 is generated under acidic conditions that are a hallmark of inflammation

Zirafi et al., 2015, Cell Reports *11*, 1–11
May 5, 2015
http://dx.doi.org/10.1016/j.celrep.2015.03.061

CellPress

Please cite this article in press as: Zirafi et al., Discovery and Characterization of an Endogenous CXCR4 Antagonist, Cell Reports (2015), http://dx.doi.org/10.1016/j.celrep.2015.03.061

Cell Reports
Article

Discovery and Characterization of an Endogenous CXCR4 Antagonist

Onofrio Zirafi,[1,18] Kyeong-Ae Kim,[1,18] Ludger Ständker,[1,2,8,18] Katharina B. Mohr,[1] Daniel Sauter,[1] Anke Heigele,[1] Silvia F. Kluge,[1] Eliza Wiercinska,[3] Doreen Chudziak,[3] Rudolf Richter,[3,17] Barbara Moepps,[4] Peter Gierschik,[4] Virag Vas,[5] Hartmut Geiger,[5] Markus Lamla,[6] Tanja Weil,[6] Timo Burster,[7] Andreas Zgraja,[8] Francois Daubeuf,[9] Nelly Frossard,[9] Muriel Hachet-Haas,[10] Fabian Heunisch,[11] Christoph Reichetzeder,[11] Jean-Luc Galzi,[10] Javier Pérez-Castells,[12] Angeles Canales-Mayordomo,[13] Jesus Jiménez-Barbero,[13] Guillermo Giménez-Gallego,[13] Marion Schneider,[14] James Shorter,[15] Amalio Telenti,[16] Berthold Hocher,[11] Wolf-Georg Forssmann,[1,8,17] Halvard Bonig,[3] Frank Kirchhoff,[1,2] and Jan Münch[1,2,*]

[1]Institute of Molecular Virology, University of Ulm, 89081 Ulm, Germany
[2]Ulm Peptide Pharmaceuticals, University of Ulm, 89081 Ulm, Germany
[3]German Red Cross Blood Service Baden-Württemberg-Hessen and Institute for Transfusion Medicine and Immunohaematology, Goethe University, 60528 Frankfurt, Germany
[4]Institute of Pharmacology and Toxicology, University of Ulm, 89081 Ulm, Germany
[5]Department of Dermatology and Allergic Diseases, University of Ulm, 89081 Ulm, Germany
[6]Institute of Organic Chemistry III, University of Ulm, 89081 Ulm, Germany
[7]Department of Neurosurgery, University of Ulm, 89081 Ulm, Germany
[8]PHARIS Biotec GmbH, 30625 Hannover, Germany
[9]UMR7200, Therapeutic Innovation Lab, CNRS-University of Strasbourg, Faculty of Pharmacy, and LabEx Medalis, 67401 Illkirch, France
[10]UMR7242, Biotechnology and Cellular Signaling, School of Biotechnology of Strasbourg, 67412 Illkirch, France
[11]Institute of Nutritional Science, University of Potsdam, 14558 Nuthetal-Potsdam, Germany
[12]Department of Chemistry, University San Pablo-CEU, 280040 Madrid, Spain
[13]Department of Physico-Chemical Biology, Centro de Investigaciones Biológicas, 28040 Madrid, Spain
[14]Experimental Anesthesiology Section, University Hospital Ulm, 89081 Ulm, Germany
[15]Department of Biochemistry and Biophysics, Perelman School of Medicine at the University of Pennsylvania, Philadelphia, PA 19104, USA
[16]J. Craig Venter Institute, La Jolla, CA 92037, USA
[17]Department of Internal Medicine, Clinic of Immunology, Hannover Medical School, 30625 Hannover, Germany
[18]Co-first author
*Correspondence: jan.muench@uni-ulm.de
http://dx.doi.org/10.1016/j.celrep.2015.03.061

SUMMARY

CXCL12-CXCR4 signaling controls multiple physiological processes and its dysregulation is associated with cancers and inflammatory diseases. To discover as-yet-unknown endogenous ligands of CXCR4, we screened a blood-derived peptide library for inhibitors of CXCR4-tropic HIV-1 strains. This approach identified a 16 amino acid fragment of serum albumin as an effective and highly specific CXCR4 antagonist. The endogenous peptide, termed EPI-X4, is evolutionarily conserved and generated from the highly abundant albumin precursor by pH-regulated proteases. EPI-X4 forms an unusual lasso-like structure and antagonizes CXCL12-induced tumor cell migration, mobilizes stem cells, and suppresses inflammatory responses in mice. Furthermore, the peptide is abundant in the urine of patients with inflammatory kidney diseases and may serve as a biomarker. Our results identify EPI-X4 as a key regulator of CXCR4 signaling and introduce proteolysis of an abundant precursor protein as an alternative concept for chemokine receptor regulation.

INTRODUCTION

CXC chemokine receptor 4 (CXCR4) is a G protein-coupled receptor (GPCR) that is expressed on multiple cells, including those of the hematopoietic and CNSs (Feng et al., 1996; Zou et al., 1998). Activation of CXCR4 by its only known chemokine ligand, stromal-cell-derived factor-1 (SDF-1 or CXCL12) (Bleul et al., 1996; Oberlin et al., 1996), governs important physiological processes, such as organogenesis, angiogenesis, migration of immune cells, and renal function, as well as retention of hematopoietic stem cells (HSCs) in the bone marrow (Petit et al., 2002; Nie et al., 2004; Chen et al., 2014). Deregulation of CXCR4/CXCL12 signaling is associated with numerous pathological conditions, including various types of cancers, chronic inflammatory diseases, cardiovascular diseases, and immunodeficiencies (Gonzalo et al., 2000; Nanki et al., 2000; Müller et al., 2001; Hernandez et al., 2003; Wen et al., 2012). Furthermore, CXCR4 serves as a major coreceptor of HIV-1 entry (Bleul et al., 1996; Oberlin et al., 1996). Thus, CXCR4 represents an interesting drug target (Choi et al., 2012; Wen et al., 2012). So

Please cite this article in press as: Zirafi et al., Discovery and Characterization of an Endogenous CXCR4 Antagonist, Cell Reports (2015), http://dx.doi.org/10.1016/j.celrep.2015.03.061

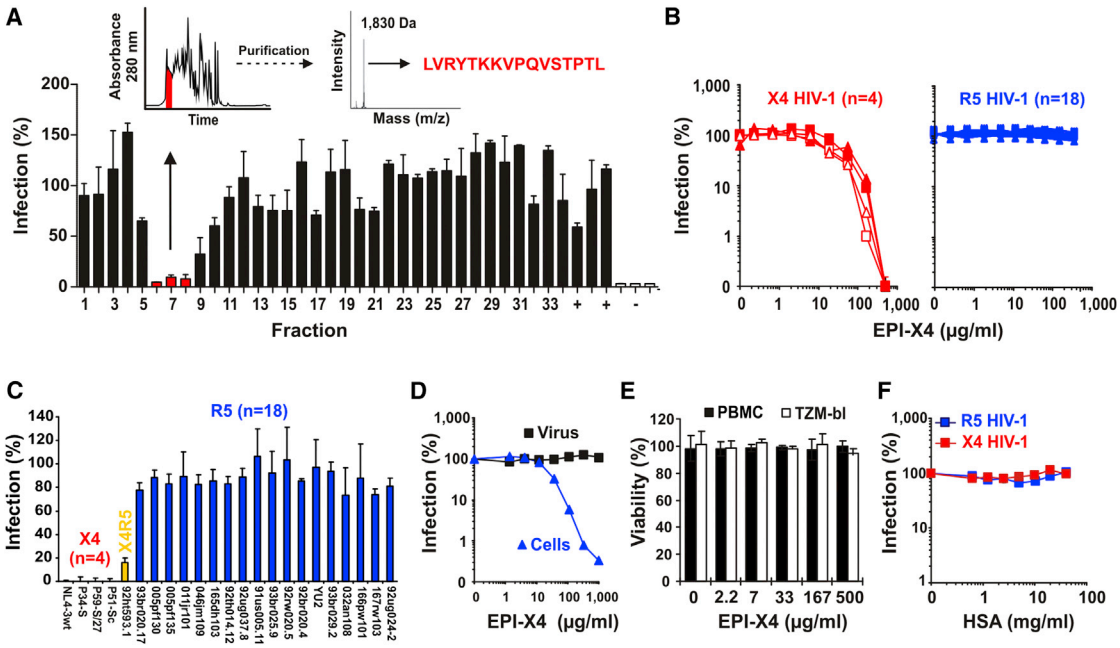

Figure 1. Identification of an Inhibitor of X4 HIV

(A) Anti-HIV activity of peptide fractions of a hemofiltrate (HF) library. +, no peptide added; −, uninfected cells. Fractions 6–8 were used for further purification and contained a 1,830 Da peptide with the indicated sequence. Values represent the mean ± SD of triplicate infections.

(B) EPI-X4 inhibits X4, but not CCR5 (R5), HIV. TZM-bl cells were infected with four X4 HIV NL4-3 constructs (left panel) or 18 CCR5-tropic derivatives thereof (Papkalla et al., 2002) (right panel) in the presence of the indicated concentrations of EPI-X4. Shown are infection rates obtained 3 days post-infection. Values represent the mean of triplicate infections (SDs are omitted for clarity).

(C) Synthetic EPI-X4 inhibits X4, but not R5, HIV-1. TZM-bl cells were infected with the indicated HIV-1 NL4-3 recombinants in the absence or presence of EPI-X4 (100 μg/ml), and infection rates were determined 3 days later. Values represent the mean ± SD of triplicate infections

(D) EPI-X4 blocks HIV-1 infection by interacting with the cell. X4 HIV-1 was pretreated with the peptide prior to infection or cells were treated with EPI-X4 and subsequently infected with HIV-1 (cells). Values represent the mean of triplicate infections.

(E) EPI-X4 is not cytotoxic. Phytohemagglutinin/IL-2-stimulated peripheral blood mononuclear cells or TZM-bl cells were incubated with the indicated concentrations of EPI-X4. After 3 days, cell viability was measured by quantifying the cell-associated ATP levels. Values represent the mean ± SD of triplicate cultures.

(F) Infection of TZM-bl cells with X4 and R5 HIV-1 in the presence of full-length HSA. Values represent the mean of triplicate infections.

See also Figure S1 and Tables S1 and S2.

far, however, only a single antagonist (plerixafor, AMD3100) has been approved for stem cell mobilization in patients who do not respond to chemotherapy or granulocyte colony-stimulating factor (G-CSF) (Devine et al., 2008).

To identify unknown endogenous CXCR4 ligands, we generated a peptide library derived from ~10,000 l of hemofiltrate (HF). This blood ultrafiltrate is obtained from dialysis centers and contains essentially the entire circulating blood peptidome with millions of compounds (Schulz-Knappe et al., 1997; Münch et al., 2014). Previously, we used this resource to discover an HIV-1 entry inhibitor that targets the viral gp41 fusion peptide (Münch et al., 2007b), and demonstrated that an optimized derivative thereof suppressed HIV-1 replication in humans (Forssmann et al., 2010). Furthermore, we identified an agonist of CCR5 (Detheux et al., 2000; Münch et al., 2002; Forssmann et al., 2010), the second main coreceptor of HIV-1 entry (Deng et al., 1996; Dragic et al., 1996). Here, we screened an HF-derived peptide library for inhibitors of CXCR4-tropic (X4) HIV-1 and identified an endogenous antagonist of CXCR4 that is generated by limited proteolysis of serum albumin, the most abundant protein in human plasma.

RESULTS

Isolation of an Endogenous Inhibitor of X4 HIV-1

The screening of 350 fractions of an HF-derived peptide library identified three adjacent peptide fractions that blocked X4-HIV-1 (Figure 1A). Further rounds of chromatographic separation and X4-HIV-1 inhibition assays (Figure S1) yielded a peptide of 1,830 Da with the amino acid sequence LVRYTKKVPQVSTPTL, which corresponds to residues 408–423 of human serum albumin (HSA) (Figure 1A). HSA is the most abundant protein in the blood, with reference concentrations between 34 and 54 g/l, and is also abundant in the extravascular space (Peters, 1996). The isolated peptide was previously detected by mass spectrometry in HF and the urine of patients with graft-versus-host and kidney disease (Kaiser et al., 2004; Chalmers et al., 2005; Wittke et al., 2005; Aristoteli et al., 2007), but its biological function remained unknown.

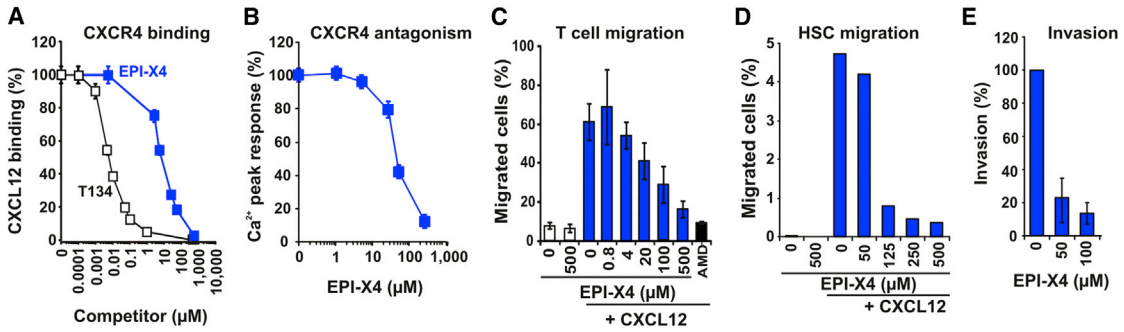

Figure 2. EPI-X4 Antagonizes CXCR4 and Suppresses CXCL12-Mediated Cellular Migration

(A) EPI-X4 and the synthetic control CXCR4 antagonist T134 inhibit binding of CXCL12 to CXCR4 in a dose-dependent manner. Each data point represents the mean ± SD of three experiments.

(B) EPI-X4 antagonizes CXCL12-mediated Ca^{2+} mobilization. HEK293 CXCR4 cells were treated with CXCL12 in the absence or presence of EPI-X4, and Ca^{2+} mobilization was monitored. Values shown are the mean Ca^{2+} peak responses from triplicate experiments relative to cells treated only with chemokine (100%).

(C) EPI-X4 blocks CXCL12-directed transwell migration of Jurkat T cells. Values shown were derived from one representative experiment performed in triplicate.

(D) EPI-X4 blocks CXCL12-induced migration of human CD34+ stem cells. Values shown were derived from one experiment performed in triplicate.

(E) The peptide blocks invasion of prostate cancer cells. Values shown were derived from one experiment performed in duplicate.

See also Figure S2.

The synthetic peptide inhibited X4-HIV-1 infection with a mean 50% inhibitory concentration (IC_{50}) of 15.8 μg/ml (corresponding to 8.6 μM) (Figure 1B; Table S1), but had no effect on CCR5- (R5) tropic HIV-1 strains (Figures 1B and 1C). Treatment of target cells, but not of virions, prevented HIV-1 infection (Figure 1D), suggesting that the peptide, named EPI-X4 (endogenous peptide inhibitor of CXCR4), targets the CXCR4 coreceptor of HIV-1 entry. EPI-X4 is not cytotoxic (Figure 1E; Table S2) and its albumin precursor exhibited no antiviral effect (Figure 1F). Thus, a naturally occurring fragment of the most abundant protein in human plasma specifically inhibits X4 HIV-1 infection.

EPI-X4 Is a Natural CXCR4 Antagonist

We next determined whether EPI-X4 interacts directly with CXCR4. EPI-X4 competed for CXCL12 binding to CXCR4 with an IC_{50} of 8.6 ± 3.1 μM, corresponding to a dissociation constant (K_i value) of 3 ± 1 μM (Figure 2A). Thus, active concentrations of this peptide can be generated by proteolytic cleavage of ~1% of its albumin precursor. The peptide also interfered with the binding of the monoclonal antibody 12G5, which interacts with the second extracellular loop of CXCR4, but had no effect on 1D9, which targets the N terminus (Figure S2A). EPI-X4 did not induce Ca^{2+} mobilization (Figure S2B) and has thus no CXCR4 agonistic activity. However, EPI-X4 inhibited CXCL12-induced Ca^{2+} mobilization (Figures 2B and S2B) and receptor internalization (Figures S2C and S2D). These effects were highly specific since EPI-X4 did not affect ligand-induced signaling via any other GPCR investigated (Figures S2B and S2E). Furthermore, EPI-X4 did not interfere with CXCL12-induced internalization of CXCR7 (Figure S2F), the alternative receptor for CXCL12 (Burns et al., 2006), and suppressed basal CXCR4 signaling (Figure S2G). Next, we examined whether EPI-X4 affects cellular migration along a CXCL12 gradient. We found that EPI-X4 inhibits CXCL12-induced migration of leukemia cells (Figure 2C) and human $CD34^+$ hematopoietic cells (Figure 2D), as well as prostate tumor cell invasion (Figure 2E). Thus, EPI-X4 is an endogenous antagonist and inverse agonist of CXCR4 that exerts anti-invasive and anti-metastatic effects.

EPI-X4 Modulates CXCR4 Signaling In Vivo

Expression of CXCL12 by bone marrow stromal cells provides a retention signal for CXCR4-expressing HSCs and neutrophils in the bone marrow. In agreement with the antagonistic activity of EPI-X4 described above, a single intraperitoneal injection of this peptide into mice resulted in marked mobilization of HSCs (Figure 3A) and neutrophils (Figure 3B) into the periphery. Notably, the mobilized cells included transplantable cells, as they engrafted lethally irradiated hosts (Figure 3C). Given that CXCR4 plays a key role in inflammation, we also examined whether EPI-X4 exerts anti-inflammatory effects in a mouse model of acute allergic airway hypereosinophilia (Reber et al., 2012). Administration of EPI-X4 prior to allergen (ovalbumin [OVA]) challenge reduced CXCR4-dependent infiltration of eosinophils, neutrophils, and lymphocytes into the airways, whereas a derivative lacking the N-terminal L (Table S1) was inactive (Figure 3D). Thus, EPI-X4 mobilizes HSCs and exerts anti-inflammatory effects in vivo.

EPI-X4 Is Evolutionarily Conserved

A physiologically relevant CXCR4 antagonist should be evolutionarily conserved. Indeed, alignment of albumin sequences from different mammalian species revealed variations at only three amino acid positions of EPI-X4: L1I/A, K6R/Q, and V8A/L (Figure 4A). Quantitative analyses confirmed that the conservation score of the region corresponding to EPI-X4 and its flanking residues (that may allow its proteolytic generation) is significantly greater (0.98) than that of the remainder of the albumin molecule (0.87; p = 0.006; Figures 4B and 4C). Importantly, substitution of the N-terminal L by I, which was observed in several species (Figure 4A), increased the activity of human EPI-X4 (Table S1). Notably, both human- and murine-derived EPI-X4 efficiently suppressed CXCL12-induced migration of

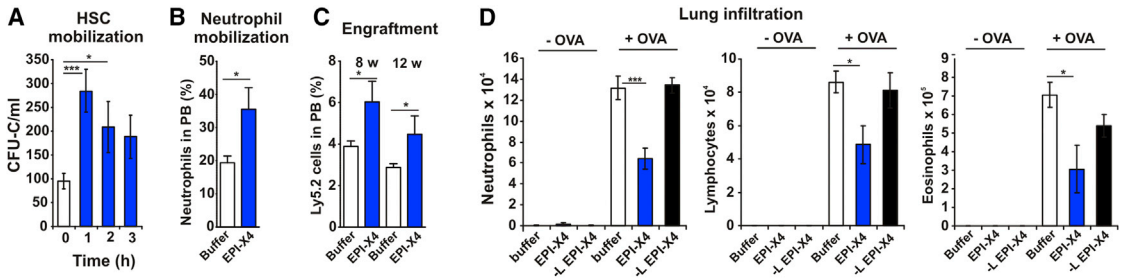

Figure 3. EPI-X4 Mobilizes Stem Cells and Inhibits Inflammation In Vivo

(A and B) Intraperitoneal administration of EPI-X4 into mice results in mobilization of clonogenic cells (CFU-C) (A) and neutrophils (B) in peripheral blood (PB). Values are mean values derived from n = 3 mice ± SEM.

(C) EPI-X4 mobilizes mouse stem cells. Multi-lineage chimerism of a donor-specific cell-surface marker (Ly5.2) in mice that were competitively transplanted with equal volumes of blood derived from mice given either EPI-X4 or saline. Values are mean values derived 8 or 12 weeks (w) after engraftment from n = 3 mice per group ± SEM.

(D) EPI-X4 inhibits inflammatory cell infiltration in a mouse model of allergic hypereosinophilia. Data are presented as means ± SEM from six mice per group. *$p < 0.05$, ***$p < 0.001$). −L EPI-X4 lacks the N-terminal leucine.

See also Table S1.

mouse cells (Figure 4D), suggesting that this endogenous CXCR4 antagonist is functionally conserved from mice to humans.

Structure and Optimization of EPI-X4

To better understand the mechanism underlying EPI-X4 function, we used NMR to solve its 3D structure (Figure 5A; Table S3). Interactions among L1, Y4, and P9 cause the backbone of the L1–P9 stretch to adopt a ring-like structure with a "tail" formed by residues V11–L16 (Figure 5B). The ring displays one highly positively charged and one strongly hydrophobic surface (Figure 5C). Computational modeling with the published CXCR4 structure (Wu et al., 2010) suggests that the positively charged face of the ring of EPI-X4 interacts with the negatively charged extracellular face of CXCR4 similarly to CXCL12 and the V3 loop of the HIV-1 gp120 exterior envelope glycoprotein (Figure S3).

Indeed, mutational analyses demonstrated that truncations of the C-terminal tail were tolerated (Figure 6A; Table S1), whereas N-terminal truncations that eliminated the ring structure resulted in a loss of activity (Figure 6B). Furthermore, substitutions of L1I (Figure 6C) and Y4W or T5S (Figure 6D) increased the antiviral activity, and combinations of these mutations (Figure 6E), including dimerization (Figure 6F), resulted in EPI-X4 derivatives with IC_{50} values in the nanomolar range (Table S1). The antiviral activity of optimized EPI-X4 derivatives correlated with their potency in inhibiting T cell migration (Figure S4A). The optimized dimeric WSC02x2 derivative also displayed strongly increased serum stability (Figure S4B), and suppressed CXCL12-induced actin polymerization in T cells (Figure S4C) and HSC migration (Figure S4D) more effectively than the parental peptide. Thus, these analyses allowed the generation of EPI-X4 derivatives with substantially increased stability and potency.

Half-Life of EPI-X4

For fast and effective regulation of CXCR4, the activity of EPI-X4 should be tightly regulated. In agreement with this requirement, the half-life of EPI-X4 spiked into plasma from healthy human individuals was only ~17 min (Figure 7A), as determined by an EPI-X4-specific sandwich ELISA (Mohr et al., 2015). Degradation and functional inactivation in plasma were blocked by L-leucinethiol (LT), an inhibitor of leucyl aminopeptidases (LAPs; Figure 7B), a group of cell-maintenance enzymes that play critical roles in the turnover of bioactive peptides and immune function (Matsui et al., 2006). These results underline the critical role of the N-terminal L-residue in the antagonistic activity of EPI-X4.

Generation of EPI-X4 from Albumin

EPI-X4 is accessible at the surface of albumin and flanked by putative protease cleavage sites (Figure S5A). We found that cathepsins D and E efficiently generated EPI-X4 from albumin under acidic conditions (Figure 7C). These aspartic proteases are major components of the endo- and lysosomal protein degradation pathway of virtually all cells (Zaidi and Kalbacher, 2008; Sun et al., 2013) and are released by exocytosis from immune cells during inflammatory processes (Yamamoto et al., 2012; Appelqvist et al., 2013). Indeed, immature dendritic cells and neutrophils supplemented with albumin produced EPI-X4 (Figure S6). Cathepsin D also circulates in an inactive form in human blood and is activated under acidic pH conditions (Tandon et al., 1990). Remarkably, we found that acidification of human plasma, which usually does not contain detectable amounts of EPI-X4 (Mohr et al., 2015), resulted in the effective de novo generation of biologically active concentrations of the CXCR4 antagonist (Figure 7D), and this process was blocked by pepstatin A, an inhibitor of aspartic proteases (Figure 7E). In agreement with a conserved regulatory role in CXCR4 signaling, EPI-X4 was also detectable in acidified sera from rhesus macaques (Figure S5B) and mice (Figure S5C). Notably, we detected higher levels of EPI-X4 in acidified sera of HIV-infected individuals with rapid disease progression (36.7 ± 9.0 μg/ml, n = 37) or chronic disease (27.9 ± 8.5 μg/ml, n = 56) than in sera obtained from elite controllers (6.3 ± 6.2 μg/ml, n = 9; Figure 7F). Thus, sera from patients with high levels of inflammation have an increased potential to generate EPI-X4. Altogether, these results suggest that EPI-X4 is effectively generated by acidic proteases present at sites of infection or inflammation, but is rapidly inactivated by serum LAP in neutral, non-inflammatory environments.

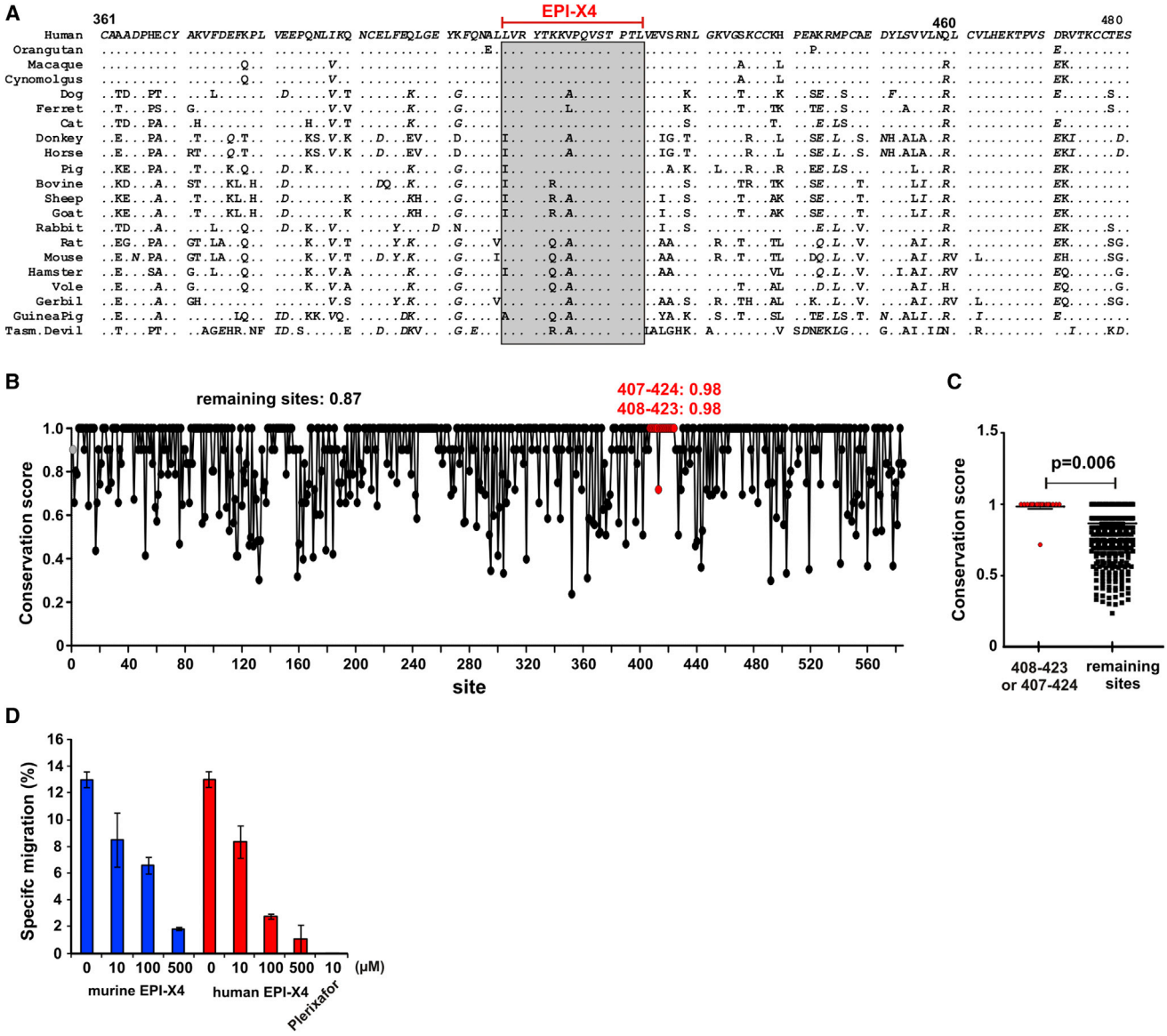

Figure 4. Structural and Functional Conservation of EPI-X4

(A) Sequence alignment of albumin proteins of the indicated species.

(B) The EPI-X4 sequence (residues 408–423) and flanking protease recognition sites (407–424) are more conserved than the remainder of the protein. Protein sequences of 21 mammalian species were aligned and residue conservation was determined using the Scorecons Server.

(C) Higher conservation of EPI-X4 and its flanking protease recognition sites (407–424) compared with the remaining sites in mammalian albumins.

(D) Murine EPI-X4 suppresses CXCL12-induced migration of mouse pro-B cells. Shown are mean values from triplicate experiments ± SD.

See also Table S1.

Urinary EPI-X4 Is a Marker for Chronic Kidney Disease

To determine whether EPI-X4 is induced under inflammatory conditions, we measured its urinary levels in patients with renal failure and in healthy controls (without prior acidification of the urine samples). High levels of EPI-X4 (1.73 ± 0.87 μg/ml, n = 12) were detected in the urine of patients with macroalbuminuria. In contrast, the levels were low in individuals with microalbuminuria (0.22 ± 0.10 μg/ml, n = 39) and essentially absent in those with no albuminuria (0.024 ± 0.004 μg/ml, n = 277; Figure 7G). Furthermore, the urinary levels of EPI-X4 were inversely correlated with the glomerular filtration rate (GFR) in these patients ($r = -0.131$, $p = 0.026$). Notably, we never observed that EPI-X4 was produced after urination, and its concentrations remained stable in urine over several days (Mohr et al., 2015). Thus, EPI-X4 is likely generated by the kidneys in vivo and its urinary levels may represent a prognostic marker for renal inflammation and chronic kidney disease.

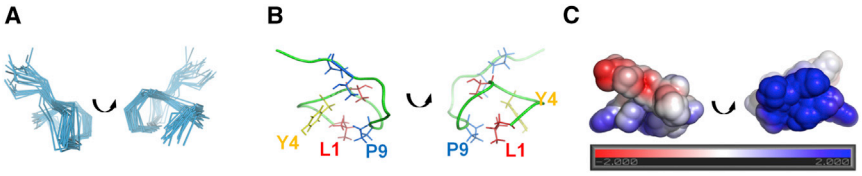

Figure 5. EPI-X4 Structure and Binding Model of CXCL12

(A) Superposition of 20 EPI-X4 conformers with the lowest final CYANA target function values.
(B) Backbone of the mean 3D structure of EPI-X4.
(C) Electrostatic potential of the surface of EPI-X4 according to the calibration bar. The images on the right were obtained after a 170° counterclockwise turn over the y axis of those on the left.
See also Figure S3 and Table S3.

DISCUSSION

In the present study, we identified EPI-X4 as an evolutionarily conserved endogenous antagonist of CXCR4 that may play important roles in physiological processes and diseases. EPI-X4 is an endogenous antagonist of a chemokine receptor that is generated from a highly abundant protein with unrelated function. The precursor, serum albumin, is ubiquitously present in intra- and extravascular compartments of the entire body with reference concentrations between 34 and 54 mg/ml (Peters, 1996). The EPI-X4-generating proteases are also available anywhere in human plasma. Thus, the "prerequisites" for rapid generation of the CXCR4 antagonist are essentially provided everywhere in the human body.

Production of EPI-X4 is likely induced by local extracellular acidification, which represents a hallmark of inflammatory tissues (Mogi et al., 2009; Dong et al., 2013; Okajima, 2013) and is emerging as a key regulatory concept for innate immunity (Rajamäki et al., 2013). Acidification results in the activation of aspartic proteases, such as cathepsins D and E, that may be secreted by lysosomal exocytosis during immune responses (Rodríguez et al., 1997; Stinchcombe et al., 2000) or via specialized secretory granules of immune cells (Levy et al., 1989; Burns et al., 2006; Yamamoto et al., 2012). Thus, EPI-X4 most likely is specifically generated at sites of infection and inflammation, and may help to trap immune cells at their places of action by preventing CXCR4-dependent migration. In addition, EPI-X4 may also be generated intracellular by lysosomal degradation of albumin (Benes et al., 2008) and subsequent release into the extracellular space after apoptosis or pyroptosis. Acidic pH values and high levels of cathepsin D are also characteristic of malignant tumors (Liaudet-Coopman et al., 2006; Benes et al., 2008; Estrella et al., 2013; Kato et al., 2013). Since EPI-X4 suppresses the migration of tumor cells, it will be of high interest to determine whether this endogenous CXCR4 antagonist may affect cancer development and tumor metastasis in vivo.

Our results support previous hypotheses that urinary EPI-X4 might serve as an early marker for renal damage, as the appearance of this peptide seems to be affected by initial changes in proteolytic activity associated with inflammatory processes at the onset of renal disease (Chalmers et al., 2005; Wittke et al., 2005). The CXCR4/CXCL12 signaling pair preserves microvascular integrity and renal function in patients with chronic kidney disease (Chen et al., 2014), and elevated levels of CXCL12 predict incident of myocardial infarction and death in these patients (Mehta et al., 2014). Thus, increased endogenous levels of EPI-X4 may represent a specific response against overshooting CXCR4 signaling. Moreover, these observations suggest that EPI-X4 or its improved derivatives have therapeutic potential in chronic kidney disease and associated disorders.

EPI-X4 was initially identified as an inhibitor of X4 HIV-1. It is tempting to speculate that the emergence of X4 HIV-1 strains during the chronic phase of infection (Connor et al., 1997) might correlate with declining concentrations of EPI-X4. However, EPI-X4 could not be detected in non-acidified plasma samples derived from HIV-1-infected individuals with late-stage disease, arguing against an essential role of EPI-X4 in the coreceptor switch. Whether or not occupancy of CXCR4 by EPI-X4 represents the long-sought "gate-keeping" mechanism that restricts sexual or perinatal transmission of X4 HIV-1 is being addressed in ongoing studies.

The finding that EPI-X4 also reduces the basal signaling activity of CXCR4 and thus acts as an inverse agonist may have important implications because it suggests that CXCR4 activity is not solely dependent on CXCL12. CXCR4 is of significant interest as a drug target (Peled et al., 2012; Cojoc et al., 2013), and EPI-X4 has interesting properties for clinical development because it mobilizes stem cells and prevents inflammatory cell infiltration in vivo. Moreover, it is not immunogenic or cytotoxic, whereas plerixafor, the only approved CXCR4 antagonist (Devine et al., 2008), affects mitochondria function (Table S2). Furthermore, EPI-X4 is functionally distinct from plerixafor because it does not bind to CXCR7 and also acts as an inverse agonist of CXCR4. Many clinically used GPCR antagonists display inverse agonist activity (Kenakin, 2004). Thus, EPI-X4 and its derivatives may be useful for the treatment of diseases associated with excessive activity of CXCR4, such as chronic inflammatory disorders and WHIM syndrome, a congenital immunodeficiency associated with increased susceptibility to human papilloma virus infection (Hernandez et al., 2003).

Our identification of an endogenous antagonist of CXCR4 signaling opens up exciting possibilities for future research. The proteolytic generation of a bioactive peptide from an abundant precursor protein represents a novel concept for the regulation of GPCRs, which are the largest and most diverse group of membrane receptors in eukaryotes and targets of almost half of all modern drugs (Lappano and Maggiolini, 2011). Our data show that this regulation of CXCR4 activity is conserved from mice to humans, and it will be interesting to determine whether other GPCRs are regulated by similar means.

EXPERIMENTAL PROCEDURES

Generation and Screening of HF Libraries

Fractions of an HF-derived peptide library (Schulz-Knappe et al., 1997) were tested for their ability to block X4 HIV-1 NL4-3 infection in P4-CCR5 cells

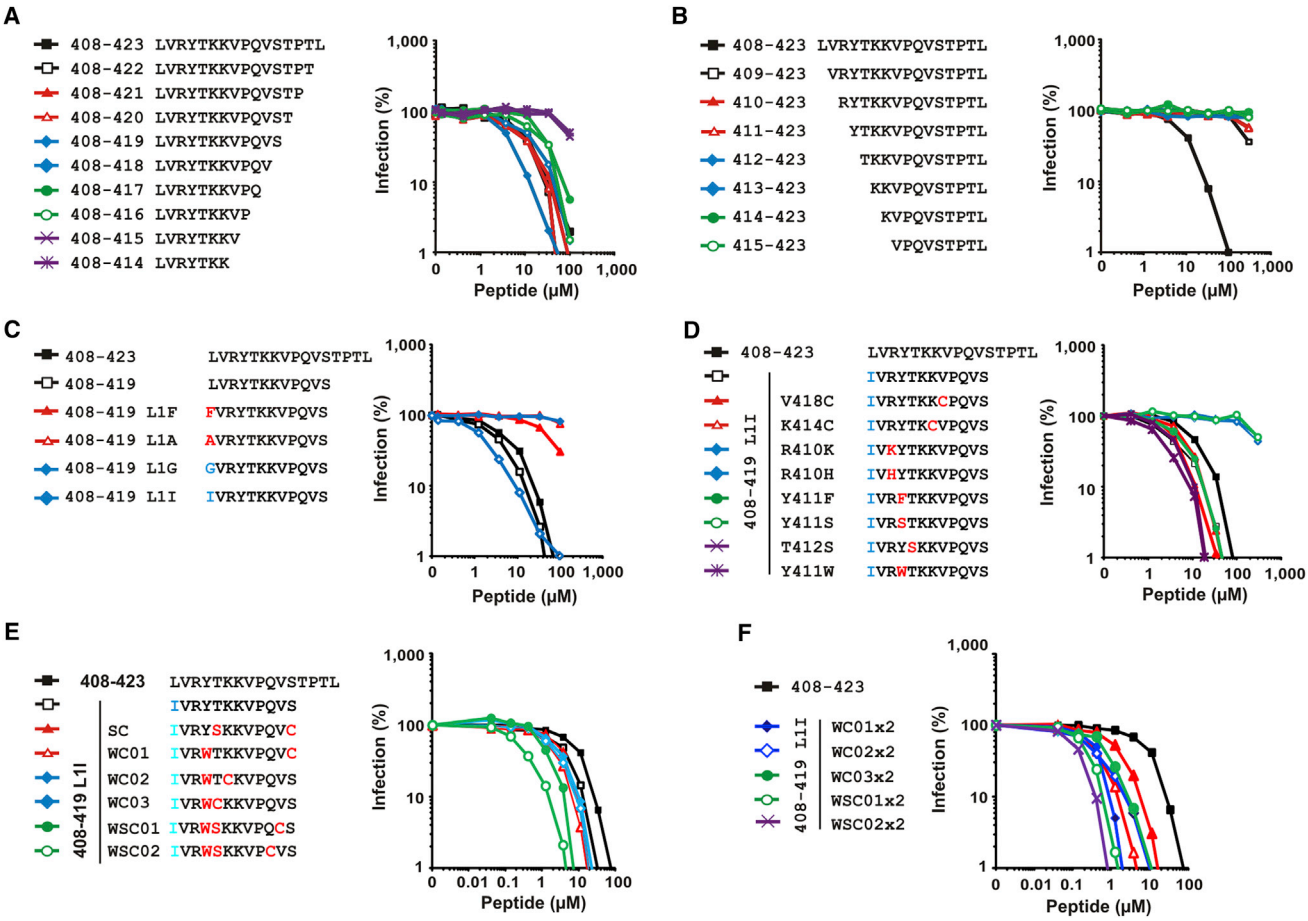

Figure 6. Antiviral Activity of EPI-X4 Derivatives against X4 HIV

(A–F) EPI-X4 (depicted as 408–423) and derivatives thereof were added to TZM-bl cells and infected with HIV-1 NL4-3. Infection rates were determined 3 days later by quantification of β-galactosidase activities. Shown are mean values from triplicate infections (bars indicating the SDs are omitted for clarity). The individual panels show the antiviral activity of C-terminal truncations of EPI-X4 (A), N-terminal truncations of EPI-X4 (B), 408–419 derivatives with substitutions at L1 (C), 408–419 L1I derivatives (D), 408–419 L1I derivatives carrying cysteines (E), and the respective dimeric mutants (F).

See also Figure S4 and Table S1.

(Münch et al., 2007b). The cells were grown in DMEM supplemented with 10% fetal calf serum (FCS) and 1 mg/ml puromycin (GIBCO BRL). Cells were seeded in flat-bottomed 96-well dishes, cultured overnight, and incubated with fractions for 2 hr before they were infected with virus containing 20 ng of p24 antigen in a total volume of 100 μl of medium. Three days after infection, the cells were lysed and infection rates were determined using the one-step Tropix Gal-Screen Kit as recommended by the manufacturer. Peptides were synthesized and the effects on HIV-1 infection in TZM-bl cells were determined as previously described (Münch et al., 2007a, 2007b). Infection rates were determined after 3 days using the one-step Tropix Gal-Screen Kit.

Real-Time Fluorescence Monitoring of Ligand-Receptor Interactions

The human chemokines CXCL12 and CXCL12-TexasRed were kindly provided by Dr. F. Baleux (Institut Pasteur, Paris, France). The synthesized T134 peptide (Tamamura et al., 1998), a small analog of T22 (a peptide derived from the polyphemusin II), was purchased from Genecust. Experiments were performed using HEK293 cells stably expressing EGFP-hCXCR4, suspended in HEPES-BSA buffer. Time-based recordings of the fluorescence emitted at 510 nm (excitation at 470 nm) were performed at 21°C with a spectrofluorometer and sampled every 0.3 s. Fluorescence binding measurements were initiated at 30 s by adding 100 nM of CXCL12-TR. For competition experiments, EGFP-CXCR4-expressing cells were preincubated for 10 min in the absence or presence of various concentrations of unlabeled T134 or EPI-X4. Subsequently, CXCL12-TR (100 nM) was added, and fluorescence was recorded until equilibrium was reached (300 s). Data were analyzed using KaleidaGraph 3.08 software (Synergy Software).

Intracellular Ca^{2+} Release Measurement

Measurements of intracellular Ca^{2+} release were carried out as previously described (Tamamura et al., 1998; Hachet-Haas et al., 2008) using indo-1 acetoxymethyl ester as the calcium probe. HEK293 cells expressing CXCR4, CCR5, or CXCR1 were preincubated for 30 min with 100 μM of EPI-X4 or buffer. Calcium release was induced by addition of their natural ligands (CXCL12, 10 nM; CCL5, 50 nM; and CXCL8, 50 nM). Cellular responses were recorded at 37°C in a 1 ml stirring cuvette with excitation set at 355 nm and emission set at 405 and 475 nm using a spectrofluorometer. Data were analyzed using KaleidaGraph 3.08 software (Synergy Software). The human chemokines CCL5, CXCL8, and CXCL11 were purchased from Clinisciences SAS.

Effect of EPI-X4 and Derivatives on Cell Migration

Migration of Jurkat cells was analyzed using 6.5-mm-diameter chambers with 5-μm-pore filters (transwell, 24-well cell culture; Costar). Jurkat cells (2×10^5)

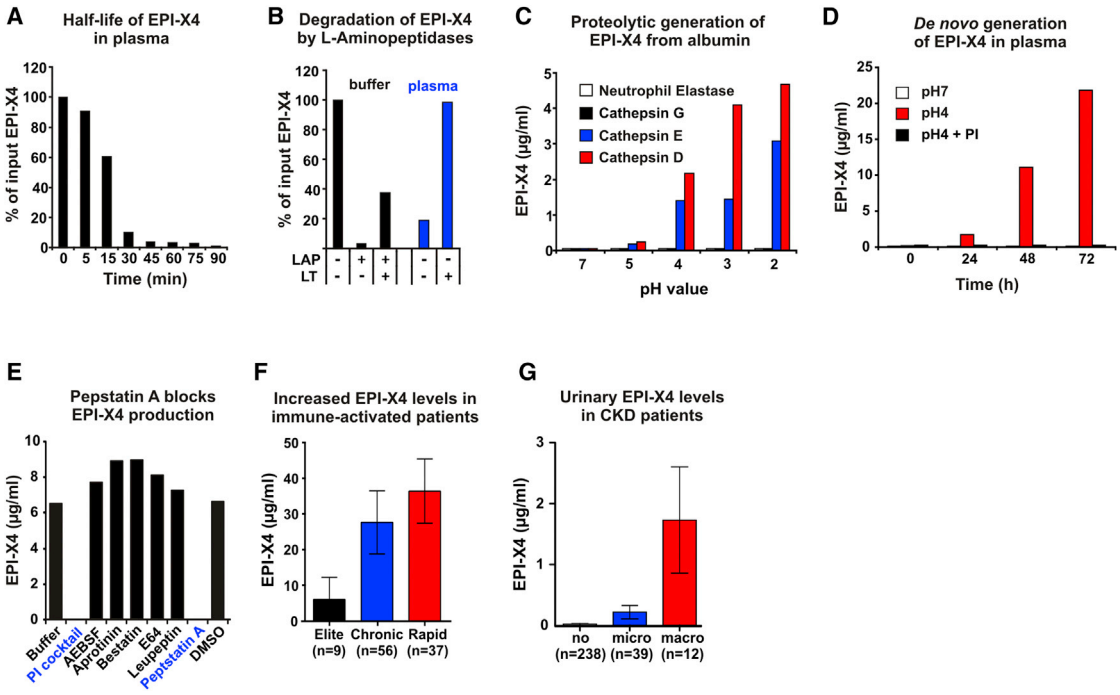

Figure 7. Degradation and Generation of EPI-X4

(A) Half-life of EPI-X4 in human plasma.

(B) EPI-X4 is degraded by recombinant or plasma leucyl aminopeptidases (LAPs). LT, L-leucinethiol (LAP inhibitor).

(C) pH-dependent generation of EPI-X4 from purified albumin by cathepsins D and E, but not neutrophil elastase or cathepsin G.

(D) Generation of EPI-X4 in acidified human plasma.

(E) The aspartyl protease inhibitor pepstatin A blocks EPI-X4 production in acidified plasma. Values shown in (A)–(E) were determined by an EPI-X4-specific sandwich ELISA and represent single data points from one representative experiment of two performed.

(F) EPI-X4 levels in acidified plasma of treatment-naive HIV-1-infected individuals.

(G) EPI-X4 concentrations in urine of patients with microalbuminuria, macroalbuminuria, or no albuminuria.

See also Figures S5 and S6.

were suspended in 200 µl of OpTmizer T Cell Expansion serum-free medium (SFM) (Life Technologies) and the cell suspensions were added to the upper chamber. Then, various concentrations of EPI-X4 or its derivatives in 600 µl T Cell Expansion SFM were added to the upper and lower chambers, and 10 nM of CXCL12 (R&D System) was added to the lower chamber. The cell-culture chambers were incubated for 150 min in a cell-culture incubator at 37°C. After incubation, chambers were removed, 100 µl of supernatants was taken, and cells that had migrated into the lower compartment were either counted directly using a hemocytometer or analyzed using the CellTiter-Glo Luminescent Cell Viability Assay (Promega). All values represent mean numbers of migrated cells relative to CXCL12-only treated cells from a triplicate experiment ± SD.

Migration of human CD34+ cells was performed using frozen CD34+ cells from G-CSF-mobilized healthy volunteer donor apheresis products from the Institute for Transfusion Medicine (University of Ulm) and the Institute for Clinical Transfusion Medicine and Immunogenetics Ulm. Cells were maintained in CellGro SCGM medium (CellGenix) supplemented with 10% FCS, 100 ng/ml rhSCF, 20 ng/ml rhIL-3, and 25 ng/ml rhIL-6. Frozen cells were carefully thawed in 1/10 diluted 10% ACD-A buffer in PBS, and 1×10^5/200 µl cells were placed into the upper chamber of transwell plates. Various concentrations of EPI-X4 were then added to the upper and lower chambers, and 10 nM CXCL12 was placed in the bottom well. After 3 hr, chemotaxis was measured using the CellTiter-Glo Luminescent Cell Viability Assay as described above. Values shown represent the mean percentage of migrated cells from one experiment performed in duplicate.

Cancer Cell Invasion

Invasion of cancer cells was assayed using a BioCoat Matrigel invasion chamber (BD) as recommended by the manufacturer. In brief, 5×10^4 DU145 cells (ATCC) were suspended in 300 µl of serum-free RPMI (GIBCO) containing 0.1% BSA (KPL) and then added to the upper chamber. Then, 700 µl serum-free medium with or without 100 nM CXCL12 and the indicated concentrations of EPI-X4 were added to each lower chamber. The chambers were incubated for 24 hr at 37°C in a humid atmosphere of 5% CO_2/95% air. The non-invading cells were removed from the upper surface of the membrane by scrubbing. Invaded cells toward the bottom of the membrane were quantified using the CellTiter-Glo Luminescent Cell Viability Assay kit as described above. Values shown are relative to those obtained for CXCL12 alone.

Progenitor Cell Mobilization in Mice

C57Bl/6J mice (Janvier) were housed in the conventional vivarium of the Goethe University Medical Center, Frankfurt, with food and water provided ad libitum. Mice received intraperitoneal (i.p.) injections of 200 µl of normal saline or normal saline containing 10 mg/ml EPI-X4. At the indicated times after injection, blood was drawn from the cheek pouch after careful skin disinfection. After hypotonic lysis of erythrocytes, leukocytes were incubated in duplicate in cytokine-replete, commercially available semisolid medium (3434, Stem Cell Technologies) under standard conditions. Colony-forming units in culture (CFU-C) were scored on day 7 as previously described (Bonig et al., 2006). CFU-C scores were normalized to the blood volume incubated and are expressed as CFU-C/ml.

Neutrophil Mobilization and Transplantation of Mobilized Cells

C57BL/6 animals were injected with EPI-X4 (2 mg i.p. in saline) or control saline. Peripheral blood cells (with the Ly5.2 [CD45.2] cell-surface phenotype) were individually harvested at 1 hr post-injection, counted (the percentage of neutrophils in peripheral blood was determined using a differential blood cell counter [Hemavet; Drew Scientific]), combined, and competitively transplanted (660 μl blood equivalent) alongside 4 × 10^5 C57BL/6 CD45.1 BM cells into C57BL/6 Cd45.1 recipients as previously described (Ryan et al., 2010). Recipient animals were subsequently analyzed for long-term multi-lineage chimerism in peripheral blood by flow cytometry.

Acute Allergic Airway Hypereosinophilia Mouse Model

On days 0, 1, and 2, mice were sensitized by i.p. injections of 50 μg OVA (A5503, Sigma-Aldrich) adsorbed on 2 mg of aluminum hydroxide (23918-6, Sigma-Aldrich) in saline. Mice were challenged by intranasal (i.n.) instillation of 10 μg OVA in 25 μl saline (12.5 μl/nostril) or saline alone for control mice on days 5, 6, and 7 under anesthesia (50 mg/kg ketamine and 3.3 mg/kg xylazine, i.p.). EPI-X4 or albumin fragment 409–423 in saline were administered i.p. (16 μmol/kg) 2 hr before each OVA challenge. Bronchoalveolar lavage (BAL) and differential cell counts were performed 24 hr after the last OVA challenge as previously described (Reber et al., 2012).

Cell Migration of Murine Pro-B Cells

Migration of murine BA/F3 pro-B cells was determined in a transwell assay as described in the Supplemental Experimental Procedures.

Degradation of EPI-X4 by LAP

In vitro degradation of EPI-X4 was performed by incubating 5 μg/ml EPI-X4 in undiluted fresh human plasma in the presence or absence of 0.05 U of LAP (L5006, Sigma-Aldrich) and 300 μM of LT (L8397, Sigma-Aldrich). Samples were incubated at 37°C for 1 hr and analyzed in an EPI-X4-specific sandwich ELISA.

Half-Life of EPI-X4 in Human Plasma

Fresh human plasma was spiked with 1 μg/ml EPI-X4 and incubated at 37°C and 5% CO_2. At the indicated times, aliquots were taken and analyzed by an EPI-X4-specific sandwich ELISA.

HSA Structure

The 3D HSA structure was downloaded from the RCSB Protein Data Bank (PDB ID: 1H9Z), and pictures were generated using PyMOL software (DeLano Scientific LLC).

Proteolytic Digestion of HSA with Cathepsins

In vitro digestion of HSA was performed by incubating 400 μg/ml of HSA (126654, Calbiochem) in the presence or absence of 10 μg/ml of cathepsin D (C8696, Sigma-Aldrich) and cathepsin E (1294-AS-010; R&D Systems) or a buffer control in 50 μl of 0.2 M citrate buffer at the indicated pH. Samples were incubated at 37°C for 4 hr and then placed on ice to stop the digestion. Samples were analyzed in an EPI-X4-specific sandwich ELISA.

De Novo Generation of EPI-X4 in Acidified Plasma

Fresh human plasma or PBS was acidified to pH 4 with 1 M of HCl. At the indicated time points, aliquots were taken and immediately stored at −80°C. The effect of a protease inhibitor (PI) cocktail (P8340, Sigma-Aldrich) on EPI-X4 generation was investigated by mixing 95% of acidified human plasma with 5% (v/v) of the protease inhibitor cocktail 1%, 5% (v/v) of DMSO (solvent), or 5% (v/v) of PBS. The effect of individual protease inhibitors was analyzed the same way. The final concentrations of individual PIs were 100 μM AEBSF (A8456, Sigma-Aldrich), 100 nM aprotinin (A1153, Sigma-Aldrich), 1 μM bestatin (B8385, Sigma), 10 μM E64 (E3132, Sigma-Aldrich), 10 μM leupeptin (L2884, Sigma-Aldrich), and 1 μM pepstatin A (P5318, Sigma-Aldrich). EPI-X4 concentrations were determined by EPI-X4-specific sandwich ELISA.

Detection of EPI-X4 in Sera from HIV-Infected Individuals

Plasma and serum from 102 HIV-infected individuals representing the full spectrum of viral load and disease progression were obtained from the Swiss HIV Cohort Study. Samples were collected while the individuals were treatment naive. See the Supplemental Experimental Procedures for details.

Detection of Urinary EPI-X4 and Correlation with the Severity of Chronic Kidney Disease

A total of 289 baseline urine samples from the Berlin Radio Contrast Media Study were analyzed (Heunisch et al., 2014). Baseline urine analyzed in this study was obtained before contrast media exposure. Patients had chronic kidney disease (stages 1–4) and clinical signs of coronary artery disease. Patients were classified according to albumin excretion (urine albumin concentrations: 0–29.9 mg/l = normal, 30–299.9 mg/l = microalbuminuria; 300–6,000 mg/l = macroalbuminuria) and impairment of GFR (stage 1: 90–120 ml/min; stage 2 60–79.9 ml/min; stage 3: 30–59.9 ml/min; stage 4: 15–29.9 ml/min). Statistical analysis was done with SPSS 20 (IBM SPSS Statistics; IBM), and $p < 0.05$ was considered statistically significant.

Statistics

Statistical analysis of the results was done using GraphPad Prism 4.0 software.

Study Approval

All mouse experiments were performed in accordance with institutional and national guidelines and regulations, and were approved by the local committees (permit AL/11/40/12/12 from the Comité Régional d'Ethique en Matière d'Expérimentation Animale de Strasbourg [N.F.] and permit F27/19 from Regierungspräsidium Darmstadt and the IACUC of Goethe University [H.B.]). All patient samples were collected and analyzed with the patient's written informed consent prior to inclusion in the study.

ACCESSION NUMBERS

The chemical shifts reported in this work have been deposited in the Biological Magnetic Resonance Bank (http://www.bmrb.wisc.edu/) and are available under accession number 25539. The atomic coordinates and structure factors or NMR restraints have been deposited in the RCSB Protein Data Bank (http://www.pdb.org) and are available under accession number 2n0x.

SUPPLEMENTAL INFORMATION

Supplemental Information includes Supplemental Experimental Procedures, six figures, and three tables and can be found with this article online at http://dx.doi.org/10.1016/j.celrep.2015.03.061.

AUTHOR CONTRIBUTIONS

O.Z. and K.-A.K. performed HIV-1 infection experiments and protease and neutrophil assays. L.S. generated libraries and purified the peptide. O.Z. and K.B.M. developed the ELISA and performed all measurements. D.S. calculated conservation scores. A.H. tested antibodies. E.W. and D.C. studied stem cell mobilization. B.M. and P.G. analyzed inverse agonism. V.V. and H.G. examined neutrophil mobilization and engraftment. M.L. and T.W. performed MALDI measurements. T.B. performed protease experiments. R.R. analyzed neutrophil supernatants. A.Z. synthesized peptides. F.D. and N.F. examined inflammatory effects in mice. M.H.-H. and J.-L.G. performed FRET assays and antagonism studies. G.S. performed mass spectrometry. J.P.-C., A.C.-M., J.J.-B., and G.G.-G. performed NMR and calculated models. A.T. provided clinical samples and data. F.B., C.R., and B.H. obtained urine samples and evaluated data. H.B., W.-G.F., F.K., and J.M. supervised the study, planned the experiments, and wrote the manuscript.

ACKNOWLEDGMENTS

We thank Rolf Kopittke and Daniela Krnavek for technical assistance. A number of reagents were obtained through the NIH AIDS Reagent Program. K.B.M. is member of the International Graduate School in Molecular Medicine Ulm (University of Ulm). This work was supported by the government

of Lower Saxony; a DFG regular research grant (MU3115/3-1) and an E-Rare/BMBF grant to J.M.; the Elisabeth-Glaser Foundation; a Gottfried-Wilhelm Leibniz award and an Advanced ERC grant to F.K.; DFG research grants BO3553/1-1 to H.B. and W.-G.F., and SCHI510/7-1 to B.S.; a Humboldt grant (DPK-422-1658/2013) to T.B.; and funds from the LABEX ANR-10-LABX-0034_Medalis to N.F. and J.-L.G. A.T. and the contributions of the Swiss HIV Cohort Study are funded by the Swiss National Science Foundation. O.Z., K.B.M., W.-G.F., F.K., and J.M. are inventors on planned, pending, or awarded patents to use EPI-X4 and its derivatives for diagnostic or therapeutic purposes.

Received: January 20, 2015
Revised: March 10, 2015
Accepted: March 25, 2015
Published: April 23, 2015

REFERENCES

Appelqvist, H., Wäster, P., Kågedal, K., and Öllinger, K. (2013). The lysosome: from waste bag to potential therapeutic target. J. Mol. Cell Biol. *5*, 214–226.

Aristoteli, L.P., Molloy, M.P., and Baker, M.S. (2007). Evaluation of endogenous plasma peptide extraction methods for mass spectrometric biomarker discovery. J. Proteome Res. *6*, 571–581.

Benes, P., Vetvicka, V., and Fusek, M. (2008). Cathepsin D—many functions of one aspartic protease. Crit. Rev. Oncol. Hematol. *68*, 12–28.

Bleul, C.C., Farzan, M., Choe, H., Parolin, C., Clark-Lewis, I., Sodroski, J., and Springer, T.A. (1996). The lymphocyte chemoattractant SDF-1 is a ligand for LESTR/fusin and blocks HIV-1 entry. Nature *382*, 829–833.

Bonig, H., Priestley, G.V., and Papayannopoulou, T. (2006). Hierarchy of molecular-pathway usage in bone marrow homing and its shift by cytokines. Blood *107*, 79–86.

Burns, J.M., Summers, B.C., Wang, Y., Melikian, A., Berahovich, R., Miao, Z., Penfold, M.E., Sunshine, M.J., Littman, D.R., Kuo, C.J., et al. (2006). A novel chemokine receptor for SDF-1 and I-TAC involved in cell survival, cell adhesion, and tumor development. J. Exp. Med. *203*, 2201–2213.

Chalmers, M.J., Mackay, C.L., Hendrickson, C.L., Wittke, S., Walden, M., Mischak, H., Fliser, D., Just, I., and Marshall, A.G. (2005). Combined top-down and bottom-up mass spectrometric approach to characterization of biomarkers for renal disease. Anal. Chem. *77*, 7163–7171.

Chen, L.-H., Advani, S.L., Thai, K., Kabir, M.G., Sood, M.M., Gibson, I.W., Yuen, D.A., Connelly, K.A., Marsden, P.A., Kelly, D.J., et al. (2014). SDF-1/CXCR4 signaling preserves microvascular integrity and renal function in chronic kidney disease. PLoS ONE *9*, e92227.

Choi, W.-T., Duggineni, S., Xu, Y., Huang, Z., and An, J. (2012). Drug discovery research targeting the CXC chemokine receptor 4 (CXCR4). J. Med. Chem. *55*, 977–994.

Cojoc, M., Peitzsch, C., Trautmann, F., Polishchuk, L., Telegeev, G.D., and Dubrovska, A. (2013). Emerging targets in cancer management: role of the CXCL12/CXCR4 axis. Onco Targets Ther *6*, 1347–1361.

Connor, R.I., Sheridan, K.E., Ceradini, D., Choe, S., and Landau, N.R. (1997). Change in coreceptor use correlates with disease progression in HIV-1—infected individuals. J. Exp. Med. *185*, 621–628.

Deng, H., Liu, R., Ellmeier, W., Choe, S., Unutmaz, D., Burkhart, M., Di Marzio, P., Marmon, S., Sutton, R.E., Hill, C.M., et al. (1996). Identification of a major co-receptor for primary isolates of HIV-1. Nature *381*, 661–666.

Detheux, M., Ständker, L., Vakili, J., Münch, J., Forssmann, U., Adermann, K., Pöhlmann, S., Vassart, G., Kirchhoff, F., Parmentier, M., and Forssmann, W.G. (2000). Natural proteolytic processing of hemofiltrate CC chemokine 1 generates a potent CC chemokine receptor (CCR)1 and CCR5 agonist with anti-HIV properties. J. Exp. Med. *192*, 1501–1508.

Devine, S.M., Vij, R., Rettig, M., Todt, L., McGlauchlen, K., Fisher, N., Devine, H., Link, D.C., Calandra, G., Bridger, G., et al. (2008). Rapid mobilization of functional donor hematopoietic cells without G-CSF using AMD3100, an antagonist of the CXCR4/SDF-1 interaction. Blood *112*, 990–998.

Dong, L., Li, Z., Leffler, N.R., Asch, A.S., Chi, J.-T., and Yang, L.V. (2013). Acidosis activation of the proton-sensing GPR4 receptor stimulates vascular endothelial cell inflammatory responses revealed by transcriptome analysis. PLoS ONE *8*, e61991.

Dragic, T., Litwin, V., Allaway, G.P., Martin, S.R., Huang, Y., Nagashima, K.A., Cayanan, C., Maddon, P.J., Koup, R.A., Moore, J.P., and Paxton, W.A. (1996). HIV-1 entry into CD4+ cells is mediated by the chemokine receptor CC-CKR-5. Nature *381*, 667–673.

Estrella, V., Chen, T., Lloyd, M., Wojtkowiak, J., Cornnell, H.H., Ibrahim-Hashim, A., Bailey, K., Balagurunathan, Y., Rothberg, J.M., Sloane, B.F., et al. (2013). Acidity generated by the tumor microenvironment drives local invasion. Cancer Res. *73*, 1524–1535.

Feng, Y., Broder, C.C., Kennedy, P.E., and Berger, E.A. (1996). HIV-1 entry cofactor: functional cDNA cloning of a seven-transmembrane, G protein-coupled receptor. Science *272*, 872–877.

Forssmann, W.-G., The, Y.H., Stoll, M., Adermann, K., Albrecht, U., Tillmann, H.C., Barlos, K., Busmann, A., Canales-Mayordomo, A., Giménez-Gallego, G., et al. (2010). Short-term monotherapy in HIV-infected patients with a virus entry inhibitor against the gp41 fusion peptide. Sci. Transl. Med. *2*, re3.

Gonzalo, J.A., Lloyd, C.M., Peled, A., Delaney, T., Coyle, A.J., and Gutierrez-Ramos, J.C. (2000). Critical involvement of the chemotactic axis CXCR4/stromal cell-derived factor-1 alpha in the inflammatory component of allergic airway disease. J. Immunol. *165*, 499–508.

Hachet-Haas, M., Balabanian, K., Rohmer, F., Pons, F., Franchet, C., Lecat, S., Chow, K.Y., Dagher, R., Gizzi, P., Didier, B., et al. (2008). Small neutralizing molecules to inhibit actions of the chemokine CXCL12. J. Biol. Chem. *283*, 23189–23199.

Hernandez, P.A., Gorlin, R.J., Lukens, J.N., Taniuchi, S., Bohinjec, J., Francois, F., Klotman, M.E., and Diaz, G.A. (2003). Mutations in the chemokine receptor gene CXCR4 are associated with WHIM syndrome, a combined immunodeficiency disease. Nat. Genet. *34*, 70–74.

Heunisch, F., von Einem, G., Alter, M., Weist, A., Dschietzig, T., Kretschmer, A., and Hocher, B. (2014). Urinary ET-1 excretion after exposure to radiocontrast media in diabetic patients and patients with preexisting mild impaired renal function. Life Sci. *118*, 440–445.

Kaiser, T., Kamal, H., Rank, A., Kolb, H.-J., Holler, E., Ganser, A., Hertenstein, B., Mischak, H., and Weissinger, E.M. (2004). Proteomics applied to the clinical follow-up of patients after allogeneic hematopoietic stem cell transplantation. Blood *104*, 340–349.

Kato, Y., Ozawa, S., Miyamoto, C., Maehata, Y., Suzuki, A., Maeda, T., and Baba, Y. (2013). Acidic extracellular microenvironment and cancer. Cancer Cell Int. *13*, 89.

Kenakin, T. (2004). Efficacy as a vector: the relative prevalence and paucity of inverse agonism. Mol. Pharmacol. *65*, 2–11.

Lappano, R., and Maggiolini, M. (2011). G protein-coupled receptors: novel targets for drug discovery in cancer. Nat. Rev. Drug Discov. *10*, 47–60.

Levy, J., Kolski, G.B., and Douglas, S.D. (1989). Cathepsin D-like activity in neutrophils and monocytes. Infect. Immun. *57*, 1632–1634.

Liaudet-Coopman, E., Beaujouin, M., Derocq, D., Garcia, M., Glondu-Lassis, M., Laurent-Matha, V., Prébois, C., Rochefort, H., and Vignon, F. (2006). Cathepsin D: newly discovered functions of a long-standing aspartic protease in cancer and apoptosis. Cancer Lett. *237*, 167–179.

Matsui, M., Fowler, J.H., and Walling, L.L. (2006). Leucine aminopeptidases: diversity in structure and function. Biol. Chem. *387*, 1535–1544.

Mehta, N.N., Matthews, G.J., Krishnamoorthy, P., Shah, R., McLaughlin, C., Patel, P., Budoff, M., Chen, J., Wolman, M., Go, A., et al.; Chronic Renal Insufficiency Cohort (CRIC) Study Investigators (2014). Higher plasma CXCL12 levels predict incident myocardial infarction and death in chronic kidney disease: findings from the Chronic Renal Insufficiency Cohort study. Eur. Heart J. *35*, 2115–2122.

Mogi, C., Tobo, M., Tomura, H., Murata, N., He, X.D., Sato, K., Kimura, T., Ishizuka, T., Sasaki, T., Sato, T., et al. (2009). Involvement of proton-sensing

TDAG8 in extracellular acidification-induced inhibition of proinflammatory cytokine production in peritoneal macrophages. J. Immunol. *182*, 3243–3251.

Mohr, K.B., Zirafi, O., Hennies, M., Wiese, S., Kirchhoff, F., and Münch, J. (2015). Sandwich enzyme-linked immunosorbent assay for the quantification of human serum albumin fragment 408-423 in bodily fluids. Anal. Biochem. *476*, 29–35.

Müller, A., Homey, B., Soto, H., Ge, N., Catron, D., Buchanan, M.E., McClanahan, T., Murphy, E., Yuan, W., Wagner, S.N., et al. (2001). Involvement of chemokine receptors in breast cancer metastasis. Nature *410*, 50–56.

Münch, J., Ständker, L., Pöhlmann, S., Baribaud, F., Papkalla, A., Rosorius, O., Stauber, R., Sass, G., Heveker, N., Adermann, K., et al. (2002). Hemofiltrate CC chemokine 1[9-74] causes effective internalization of CCR5 and is a potent inhibitor of R5-tropic human immunodeficiency virus type 1 strains in primary T cells and macrophages. Antimicrob. Agents Chemother. *46*, 982–990.

Münch, J., Rücker, E., Ständker, L., Adermann, K., Goffinet, C., Schindler, M., Wildum, S., Chinnadurai, R., Rajan, D., Specht, A., et al. (2007a). Semen-derived amyloid fibrils drastically enhance HIV infection. Cell *131*, 1059–1071.

Münch, J., Ständker, L., Adermann, K., Schulz, A., Schindler, M., Chinnadurai, R., Pöhlmann, S., Chaipan, C., Biet, T., Peters, T., et al. (2007b). Discovery and optimization of a natural HIV-1 entry inhibitor targeting the gp41 fusion peptide. Cell *129*, 263–275.

Münch, J., Ständker, L., Forssmann, W.-G., and Kirchhoff, F. (2014). Discovery of modulators of HIV-1 infection from the human peptidome. Nat. Rev. Microbiol. *12*, 715–722.

Nanki, T., Hayashida, K., El-Gabalawy, H.S., Suson, S., Shi, K., Girschick, H.J., Yavuz, S., and Lipsky, P.E. (2000). Stromal cell-derived factor-1-CXC chemokine receptor 4 interactions play a central role in CD4+ T cell accumulation in rheumatoid arthritis synovium. J. Immunol. *165*, 6590–6598.

Nie, Y., Waite, J., Brewer, F., Sunshine, M.-J., Littman, D.R., and Zou, Y.-R. (2004). The role of CXCR4 in maintaining peripheral B cell compartments and humoral immunity. J. Exp. Med. *200*, 1145–1156.

Oberlin, E., Amara, A., Bachelerie, F., Bessia, C., Virelizier, J.L., Arenzana-Seisdedos, F., Schwartz, O., Heard, J.M., Clark-Lewis, I., Legler, D.F., et al. (1996). The CXC chemokine SDF-1 is the ligand for LESTR/fusin and prevents infection by T-cell-line-adapted HIV-1. Nature *382*, 833–835.

Okajima, F. (2013). Regulation of inflammation by extracellular acidification and proton-sensing GPCRs. Cell. Signal. *25*, 2263–2271.

Papkalla, A., Münch, J., Otto, C., and Kirchhoff, F. (2002). Nef enhances human immunodeficiency virus type 1 infectivity and replication independently of viral coreceptor tropism. J. Virol. *76*, 8455–8459.

Peled, A., Wald, O., and Burger, J. (2012). Development of novel CXCR4-based therapeutics. Expert Opin. Investig. Drugs *21*, 341–353.

Peters, T. (1996). All About Albumin: Biochemistry, Genetics and Medical Applications (San Diego, CA: Academic Press Limited).

Petit, I., Szyper-Kravitz, M., Nagler, A., Lahav, M., Peled, A., Habler, L., Ponomaryov, T., Taichman, R.S., Arenzana-Seisdedos, F., Fujii, N., et al. (2002). G-CSF induces stem cell mobilization by decreasing bone marrow SDF-1 and up-regulating CXCR4. Nat. Immunol. *3*, 687–694.

Rajamäki, K., Nordström, T., Nurmi, K., Åkerman, K.E., Kovanen, P.T., Öörni, K., and Eklund, K.K. (2013). Extracellular acidosis is a novel danger signal alerting innate immunity via the NLRP3 inflammasome. J. Biol. Chem. *288*, 13410–13419.

Reber, L.L., Daubeuf, F., Nemska, S., and Frossard, N. (2012). The AGC kinase inhibitor H89 attenuates airway inflammation in mouse models of asthma. PLoS ONE *7*, e49512.

Rodríguez, A., Webster, P., Ortego, J., and Andrews, N.W. (1997). Lysosomes behave as Ca2+-regulated exocytic vesicles in fibroblasts and epithelial cells. J. Cell Biol. *137*, 93–104.

Ryan, M.A., Nattamai, K.J., Xing, E., Schleimer, D., Daria, D., Sengupta, A., Köhler, A., Liu, W., Gunzer, M., Jansen, M., et al. (2010). Pharmacological inhibition of EGFR signaling enhances G-CSF-induced hematopoietic stem cell mobilization. Nat. Med. *16*, 1141–1146.

Schulz-Knappe, P., Schrader, M., Ständker, L., Richter, R., Hess, R., Jürgens, M., and Forssmann, W.G. (1997). Peptide bank generated by large-scale preparation of circulating human peptides. J. Chromatogr. A *776*, 125–132.

Stinchcombe, J.C., Page, L.J., and Griffiths, G.M. (2000). Secretory lysosome biogenesis in cytotoxic T lymphocytes from normal and Chediak Higashi syndrome patients. Traffic *1*, 435–444.

Sun, H., Lou, X., Shan, Q., Zhang, J., Zhu, X., Zhang, J., Wang, Y., Xie, Y., Xu, N., and Liu, S. (2013). Proteolytic characteristics of cathepsin D related to the recognition and cleavage of its target proteins. PLoS ONE *8*, e65733.

Tamamura, H., Xu, Y., Hattori, T., Zhang, X., Arakaki, R., Kanbara, K., Omagari, A., Otaka, A., Ibuka, T., Yamamoto, N., et al. (1998). A low-molecular-weight inhibitor against the chemokine receptor CXCR4: a strong anti-HIV peptide T140. Biochem. Biophys. Res. Commun. *253*, 877–882.

Tandon, A.K., Clark, G.M., Chamness, G.C., Chirgwin, J.M., and McGuire, W.L. (1990). Cathepsin D and prognosis in breast cancer. N. Engl. J. Med. *322*, 297–302.

Wen, J., Zhang, J.-Q., Huang, W., and Wang, Y. (2012). SDF-1α and CXCR4 as therapeutic targets in cardiovascular disease. Am J Cardiovasc Dis *2*, 20–28.

Wittke, S., Mischak, H., Walden, M., Kolch, W., Rädler, T., and Wiedemann, K. (2005). Discovery of biomarkers in human urine and cerebrospinal fluid by capillary electrophoresis coupled to mass spectrometry: towards new diagnostic and therapeutic approaches. Electrophoresis *26*, 1476–1487.

Wu, B., Chien, E.Y., Mol, C.D., Fenalti, G., Liu, W., Katritch, V., Abagyan, R., Brooun, A., Wells, P., Bi, F.C., et al. (2010). Structures of the CXCR4 chemokine GPCR with small-molecule and cyclic peptide antagonists. Science *330*, 1066–1071.

Yamamoto, K., Kawakubo, T., Yasukochi, A., and Tsukuba, T. (2012). Emerging roles of cathepsin E in host defense mechanisms. Biochim. Biophys. Acta *1824*, 105–112.

Zaidi, N., and Kalbacher, H. (2008). Cathepsin E: a mini review. Biochem. Biophys. Res. Commun. *367*, 517–522.

Zou, Y.R., Kottmann, A.H., Kuroda, M., Taniuchi, I., and Littman, D.R. (1998). Function of the chemokine receptor CXCR4 in haematopoiesis and in cerebellar development. Nature *393*, 595–599.

Cell Reports

Supplemental Information

Discovery and Characterization of an Endogenous CXCR4 Antagonist

Onofrio Zirafi, Kyeong-Ae Kim, Ludger Ständker, Katharina B. Mohr, Daniel Sauter, Anke Heigele, Silvia F. Kluge, Eliza Wiercinska, Doreen Chudziak, Rudolf Richter, Barbara Moepps, Peter Gierschik, Virag Vas, Hartmut Geiger, Markus Lamla, Tanja Weil, Timo Burster, Andreas Zgraja, Francois Daubeuf, Nelly Frossard, Muriel Hachet-Haas, Fabian Heunisch, Christoph Reichetzeder, Jean-Luc Galzi, Javier Pérez-Castells, Angeles Canales-Mayordomo, Jesus Jiménez-Barbero, Guillermo Giménez-Gallego, Marion Schneider, James Shorter, Amalio Telenti, Berthold Hocher, Wolf-Georg Forssmann, Halvard Bonig, Frank Kirchhoff, and Jan Münch

Supplemental Information

Supplemental Figures

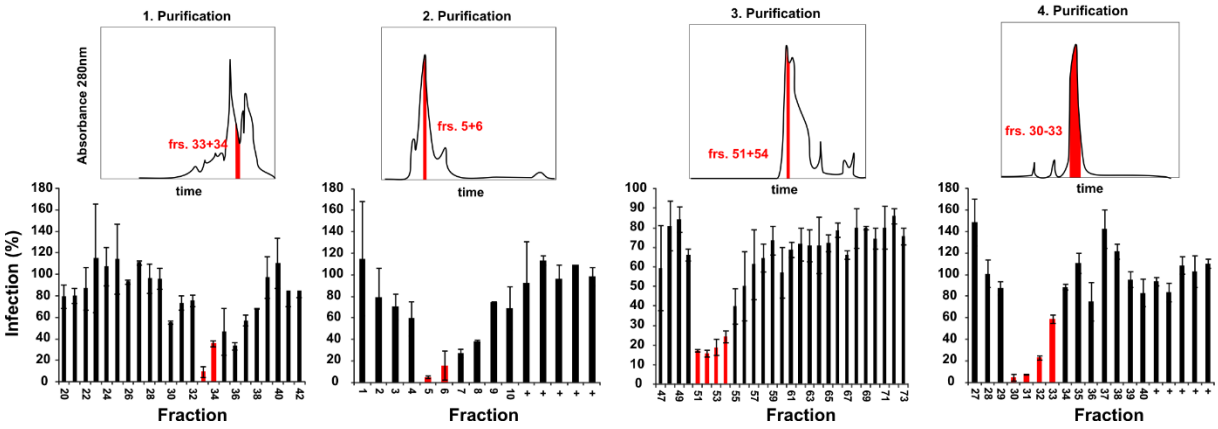

Figure S1. Purification of an inhibitor of X4 HIV from hemofiltrate, Related to Figure 1. HIV inhibitory fractions 6-8 of the initial screen (see Figure 1A) were pooled and chromatographically separated (1st purification) and the resulting fractions were tested in the HIV infection assay in P4-CCR5 cells. Inhibiting fractions 33 and 34 of this run were pooled again, purified and tested (2nd purification). After two more rounds of anti-HIV assays and fractionation, fraction 30 obtained after the fourth purification step was subjected to mass spectrometry, and its peptide sequence was determined by Edman degradation (see Figure 1A).

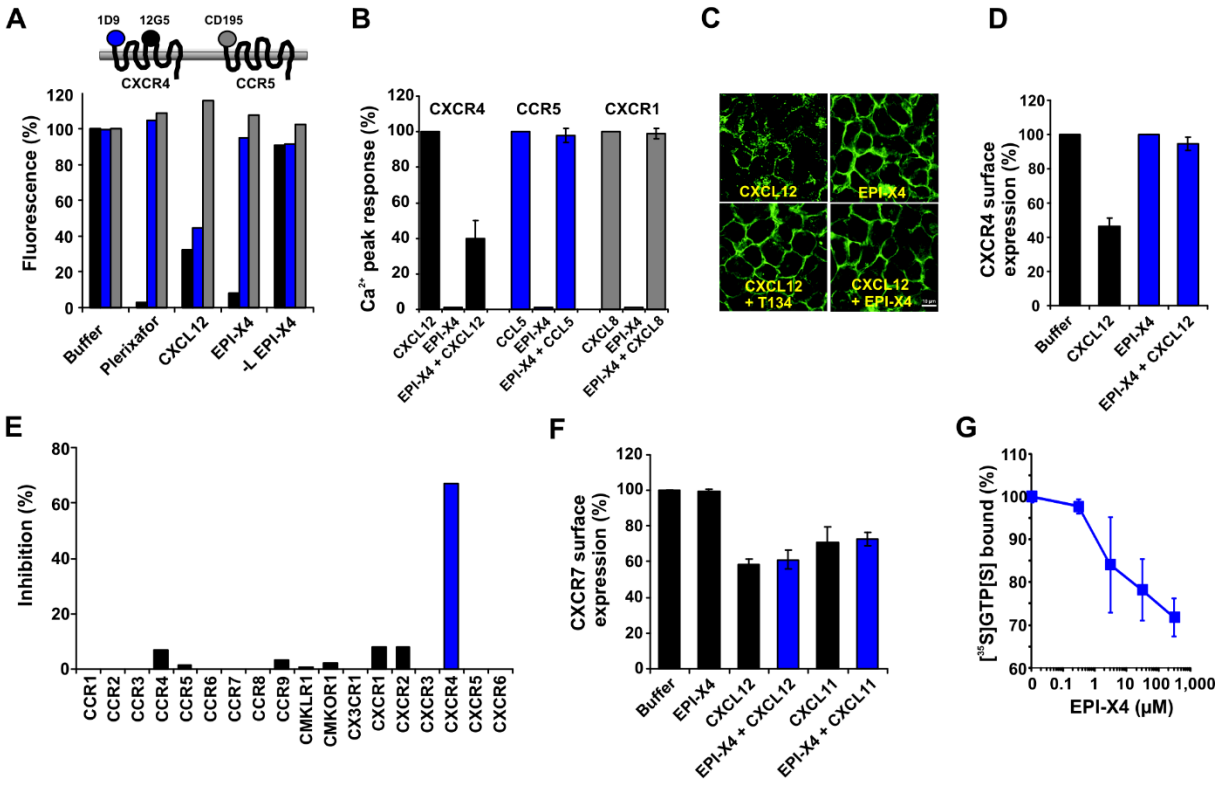

Figure S2. EPI-X4 binds and antagonizes CXCR4, Related to Figure 2.

(A) EPI-X4 interferes with binding of the 12G5 antibody to CXCR4. GHOST-CXCR4 cells were incubated with indicated compounds and stained with CXCR4-specific antibodies 1D9 and 12G5, or GHOST-CXCR5 cells were treated the same way but using the CCR5-specific antibody CD195. Antibody binding was assayed by flow cytometry. (B) EPI-X4 specifically blocks signaling of CXCL12 via CXCR4. HEK 293 cells expressing CXCR4, CCR5 or CXCR1 were treated with CXCL12, CCL5 or CXCL8 ligands, and EPI-X4 alone, or a combination thereof, and Ca^{2+} mobilization was monitored. Shown are mean values ± SD derived from triplicate measurements. (C) Confocal microscopy images of GFP-CXCR4 surface expression on HEK293 cells after treatment with CXCL12 and/or EPI-X4. Scale bar: 10 µm. (D) Flow cytometric analysis of the cells shown in (C) with the 1D9 antibody. (E) EPI-X4 specifically blocks ß-arrestin-recruitment via CXCR4. (F) EPI-X4 does not antagonize CXCR7 internalization mediated by CXCL12 or CXCL11. Values show in (D) and (F) are mean internalization responses from triplicate experiments ± SD relative to cells treated only with buffer (100%). (G) EPI-X4 reduces basal CXCR4 signaling in the absence of CXCL12. Shown are average values (± SD) derived from triplicate determinations.

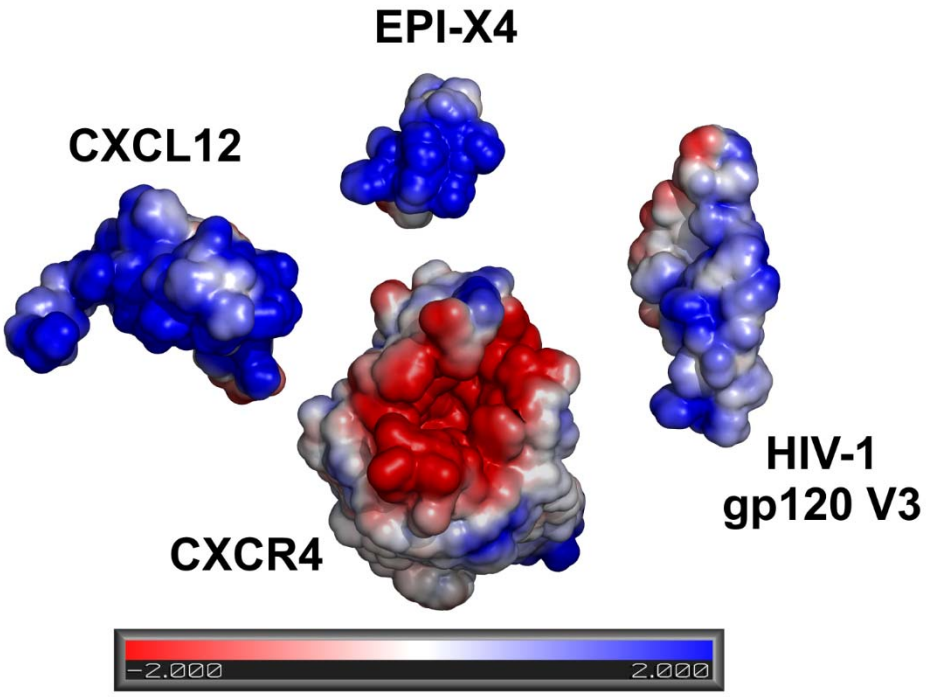

Figure S3. EPI-X4 and the V3 loop of gp120 to CXCR4, Related to Figure 5. The electrostatic potential (kbTec-1) of CXCR4 facing the extracellular space and its natural ligands are shown (CXCR4 and CXCL12 adapted from reference (Wu *et al.*, 2010)).

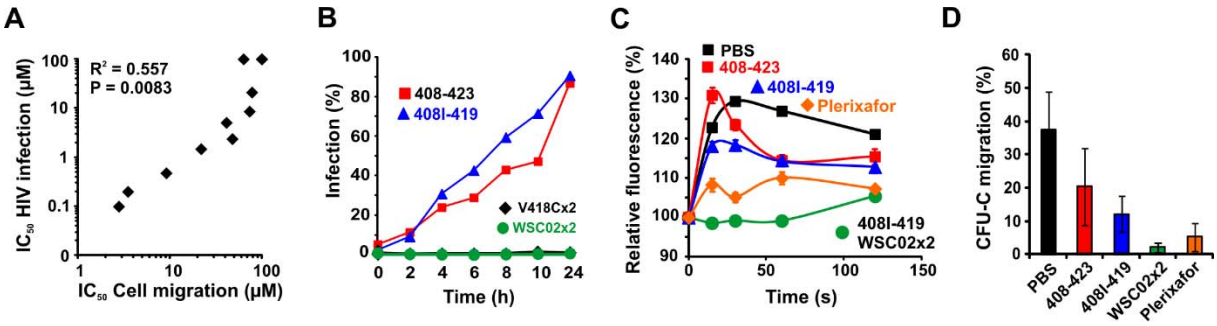

Figure S4. Optimized EPI-X4 derivatives are effective CXCR4 antagonists, Related to Figure 6. (A) EPI-X4 derivatives with increased anti-HIV activity are more potent inhibitors of CXCL12 mediated T-cell migration. The half-maximal inhibitory activity (IC_{50}) of 10 EPI-X4 derivatives to block T-cell migration towards CXCL12 was determined and correlated with the respective IC_{50} values obtained in HIV infection experiments. (B) Antiviral activity of dimeric EPI-X4 derivatives incubated in human serum. (C) The 408I-419WSC02x2 derivative is a potent inhibitor of CXCL12-induced actin polymerization in T cells. Mean F-actin fluorescence intensities are shown relative to the unstimulated control (100%; mean ± SEM, n≥3 for all conditions). (D) Optimized EPI-X4 derivatives block CXCL12-induced stem cell migration. Data derived from three independent experiments are expressed as migrated CFU-C relative to total input CFU-C (in %) ± SEM. (CFU, colony forming units). EPI-X4 is depicted as ALB408-423.

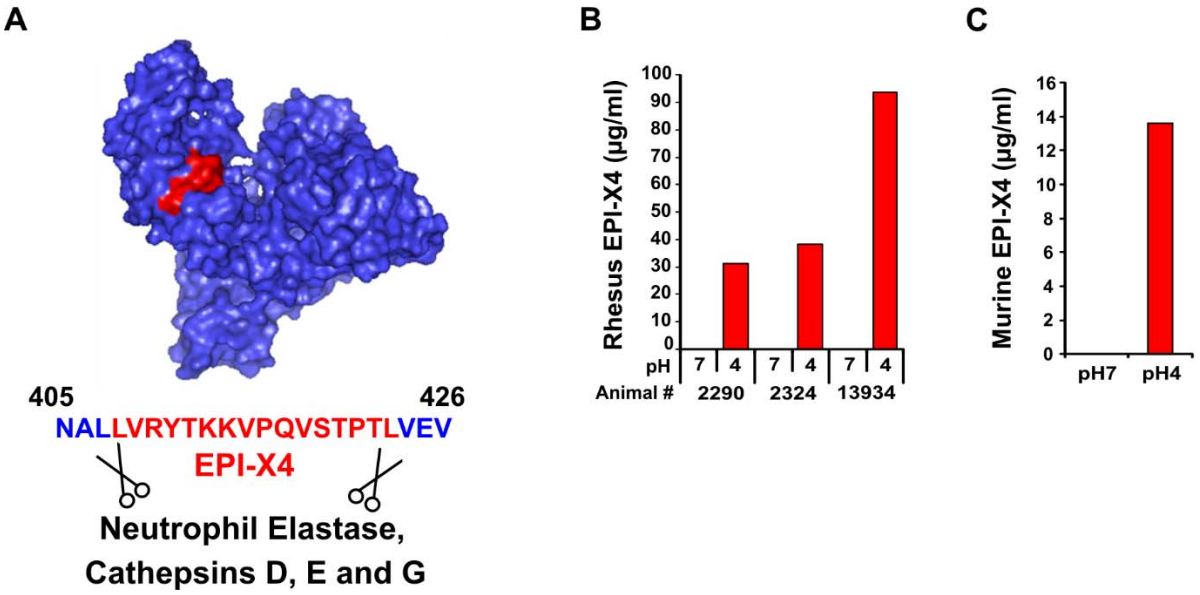

Figure S5. Putative protease restriction sites in HSA and evolutionary conservation of EPI-X4, Related to Figure 4 and 7. (A) Localization of EPI-X4 (red) within the albumin molecule (blue). (B, C) Generation of rhesus and murine EPI-X4 by acidification of sera derived from or sera from three individual rhesus macaques (B) or pooled mouse serum (C).

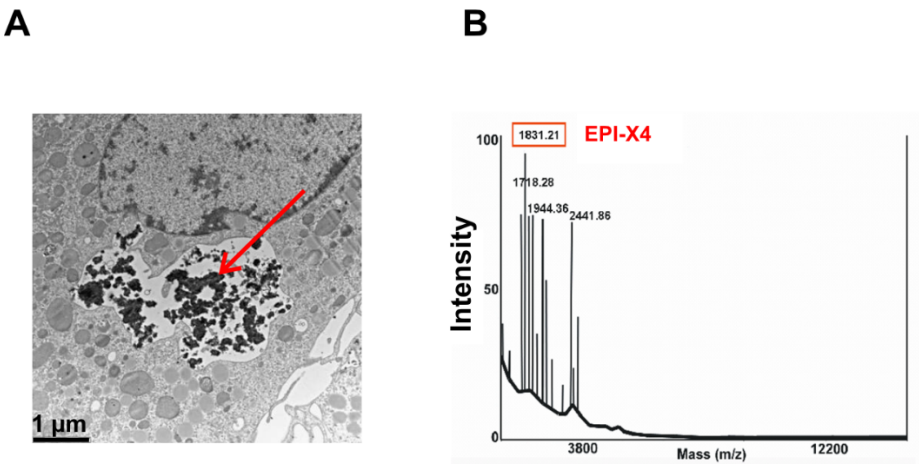

Figure S6. Engulfment of albumin and production of EPI-X4 by immune cells, Related to Figure 7. (A) iDC (immature dendritic cells) treated with 0.5% human serum albumin for 3 days accumulate the protein in large endosomal structures (indicated by red arrow). Such endosomes with this type of content have not been observed in iDC cultures which have not been treated with albumin. (B) Activated neutrophils release proteases that generate EPI-X4 from HSA. Neutrophils were incubated with human serum albumin, and samples were taken at 0, 1, 5, 10, 20, 60, 120, and 180 min. Subsequently, the samples were chromatographed on a reverse phase column, and collected fractions were analyzed by MALDI mass spectrometry. The Mr of 1,831.21, correlating with the theoretical average Mr 1,830.2 of EPI-X4, was detected in the sample obtained after 10 min. EPI-X4 was identified by sequence analysis by ESI-MSMS.

Table S1. Antiviral activity of EPI-X4 derivatives against X4 HIV NL4-3, Related to Figure 1, 3, 4 and 6. IC_{50} values were obtained from at least two independent experiments performed in triplicate. MW, molecular weight.

Derivative	Sequence	MW	IC_{50} (µM)
408-423	LVRYTKKVPQVSTPTL	1,830	8.63
415-423	VPQVSTPTL	941	>100
414-423	KVPQVSTPTL	1,068	>100
413-423	KKVPQVSTPTL	1,196	>100
412-423	TKKVPQVSTPTL	1,298	>100
411-423	YTKKVPQVSTPTL	1,461	>100
410-423	RYTKKVPQVSTPTL	1,618	>100
409-423	VRYTKKVPQVSTPTL	1,717	>100
408-422	LVRYTKKVPQVSTPT	1,720	13.4
408-421	LVRYTKKVPQVSTP	1,619	14.0
408-420	LVRYTKKVPQVST	1,522	15.3
408-419	LVRYTKKVPQVS	1,422	5.49
408-418	LVRYTKKVPQV	1,334	26.8
408-417	LVRYTKKVPQ	1,232	19.8
408-415	LVRYTKKV	1,006	>100
408-414	LVRYTKK	907	>100
408-413	LVRYTK	779	>100
408I-419	IVRYTKKVPQVS	1,421	2.48
408F-419	FVRYTKKVPQVS	1,454	92.8
408A-419	AVRYTKKVPQVS	1,378	>100
408G-419	GVRYTKKVPQVS	1,366	>100
408I-419R410H	IVHYTKKVPQVS	1,399	>100
408I-419R410K	IVKYTKKVPQVS	1,390	>100
408I-419Y411F	IVRFTKKVPQVS	1,399	3.89
408I-419Y411S	IVRSTKKVPQVS	1,342	>100
408I-419Y411W	IVRWTKKVPQVS	1,441	1.54
408I-419T412S	IVRYSKKVPQVS	1,404	2.09
408I-419K414C	IVRYTKCVPQVS	1,393	5.87
408I-419V418C	IVRYTKKVPQCS	1,421	3.69
408I-418SC	IVRYSKKVPQC	1,320	2.94
408I-419WC01	IVRWTKKVPQVC	1,456	1.65
408I-419WC02	IVRWTCKVPQVS	1,415	2.10
408I-419WC03	IVRWCKKVPQVS	1,442	1.82
408I-419WSC01	IVRWSKKVPQCS	1,430	0.87
408I-419WSC02	IVRWSKKVPCVS	1,401	0.31
408I-419WSC03	IVRWSKKVCQVS	1,432	1.51
408I-419K414Cx2	(IVRYTKCVPQVS)x2	2,783	1.05
408I-419V418Cx2	(IVRYTKKVPQCS)x2	2,842	0.46
408I-419WC01x2	(IVRWTKKVPQVC)x2	2,911	0.40
408I-419WC02x2	(IVRWTCKVPQVS)x2	2,829	0.32
408I-419WC03x2	(IVRWCKKVPQVS)x2	2,883	0.60
408I-418SCx2	(IVRYSKKVPQC)x2	2,639	0.39
408I-419WSC01x2	(IVRWSKKVPQCS)x2	2,859	0.18
408I-419WSC02x2	(IVRWSKKVPCVS)x2	2,801	0.12

Table S2. Cytotoxicity screening panel of Plerixafor and EPI-X4 derivatives, Related to Figure 1.

	Plerixafor	**EPI-X4**	**408I-419**	**408I-419 WSC02x2**	**409-423**
C-max	100 μM	400 μM	400 μM	400 μM	400 μM
Cell count	NR	NR	NR	NR	NR
Nuclear size	NR	NR	NR	NR	NR
DNA structure	NR	NR	NR	NR	NR
Cell membrane permeability	NR	NR	NR	NR	NR
Mitochondrial membrane potential	**21.0 μM↓**	NR	NR	NR	NR
Mitochondrial mass	**25.9 μM↑**	NR	NR	NR	NR
Cytochrome c	**18.8 μM↓**	NR	NR	NR	NR

C-max = Highest concentration tested.

Other values give the minimum effective concentration that significantly crossed the vehicle control threshold.

↓ ↑= Direction of response.

NR = No response observed.

Table S3. Long-distance NOEs between the residues of the hydrophobic core of EPI-X4, Related to Figure 5.

First atom	Second atom	Distance Å	Viol. Å (No. St)
QD2 LEU 1	HB3 PRO 9	2.85	0.01 (3)
QD2 LEU 1	HB2 PRO 9	3.76	0 (0)
QD1 LEU 1	HB3 PRO 9	3.84	0 (1)
QD1 LEU 1	HG3 PRO 9	3.91	0 (0)
QD TYR4	HD3 PRO9	5.11	0 (0)
QD TYR4	HG2 PRO9	5.5	0 (0)
QE TYR4	HG2 PRO9	5.14	0 (1)
QD TYR4	HB3 PRO9	5.5	0 (0)
QD TYR4	QG2 THR13	5.2	0 (0)
QD TYR4	QG2 THR13	5.5	0 (0)
QG2 THR 5	QG2 THR 13	3.05	0.02 (3)
QG2 THR 5	QG2 THR 13	3.05	0.02 (3)
HA THR 5	HD3 PRO 14	3.37	0 (0)
HB THR 5	HD2 PRO 14	3.86	0 (0)
QG2 THR 5	HD3 PRO 14	3.87	0 (1)
HB THR 5	HD2 PRO 14	3.82	0 (1)
QG2 THR 5	HD3 PRO 14	3.87	0 (1)
HA THR 5	HD3 PRO 14	3.54	0 (0)

Supplemental Experimental Procedures

Cell viability and Cytotoxicity. TZM-bl cells or prestimulated PBMC were incubated with increasing concentrations of peptides. Cell viability was determined using the CellTiter-Glo Luminescent Cell Viability Assay (PROMEGA, G7571) as recommended by the manufacturer. Values were derived from triplicate measurements. Vitality rates were calculated relative to ATP levels in PBS (no peptide) containing cells (100%). Data were recorded using an Orion plate luminometer 10 min after adding the reagent. The effect of Plerixafor (Calbiochem) and indicated EPI-X4 derivatives on cell loss, nuclear size, nuclear morphology, cell membrane permeability, mitochondrial membrane potential, mitochondrial mass and cytochrome c release was performed by Cyprotex (Macclesfield, UK) using HepG2 cells as described (O'Brien *et al.*, 2006) (www.cyprotex.com/toxicology/multiparametric/cytotoxicity-screening-panel/). Briefly, HepG2 cells were treated with serial dilutions of Plerixafor (8-point dose-response curve up to 100 μM), EPI-X4 peptides (8-point dose-response curve up to 400 μM) and 0.5% DMSO as vehicle control, and chlorpromazine and valinomycin as positive controls. Toxicity markers were quantified using Cellomics ArrayScan® VTI or Cellomics ToxInsight (Thermo Scientific) using 3 replicates per concentration.

EPI-X4 interaction with CXCR4 on GHOST cells. The binding site of EPI-X4 on CXCR4 was assessed by flow cytometry analysis (FACSCalibur; Becton Dickinson) of GHOST-CXCR4 cells (NIH & AIDS Research and Reference Reagent Program), using anti-human CXCR4 mAbs 12G5 or 1D9 (BD Pharmingen), and a CCR5 mAb (BD Pharmingen, clone: CD195) as control. GHOST cells were harvested using Cell Dissociation Solution (Non-enzymatic 1x; Sigma). 1 x 10^5 GHOST cells were incubated with CXCL12 (100 nM), Plerixafor (100 nM) or EPI-X4 peptides (100 μM) for 30 min at 4°C in serum-free medium. After incubation, cells were washed with FACS buffer (PBS + 1% FCS) by centrifugation, then sequentially stained with either PE-labeled anti-human CXCR4 mAb or CCR5 mAb at 4°C. After being washed, the cells were fixed with 4% paraformaldehyde in FACS buffer for 5 min at 4°C and then analyzed on a flow cytometer. Data were processed using CELLQUEST (Becton Dickinson).

Internalization of EGFP-CXCR4 or EGFP-CXCR7. The human CXCR7 cDNA was cloned in fusion with EGFP-cDNA into a modified pIRES Hyg 3 vector (Clonetech). HEK 293T cells stably expressing EGFP-CXCR7 were generated by the calcium phosphate-DNA co-precipitation method. Internalization of receptors was carried out as described (Hachet-Haas *et al.*, 2008). Briefly, HEK 293 cells expressing EGFP-CXCR4 or CXCR7 were pre-incubated for 30 min at 37°C with EPI-X4 (50 μM) or buffer. Thereafter, 100 nM of CXCL12 or CXCL11 were added, and 15 min later, the cell suspension was collected and labeled at the cell surface with a monoclonal mouse anti-GFP (Roche Molecular Biochemicals; 1/100 dilution) as primary antibody and a R-PE-conjugated AffiniPure F(ab′)$_2$ fragment goat anti-mouse IgG (Immunotech; 1/100) as secondary antibody. The proportion of chemokine receptors at the cell surface was directly correlated to the ratio of the PE fluorescence intensity with chemokine to that without chemokine. CXCR4 or CXCR7 staining was quantified by flow cytometric analysis (10,000 cells per sample) on a cytometer (FACScalibur, Becton-Dickinson). Mean of CXCR4 or CXCR7 fluorescence intensity was calculated using CELLQuest (Becton-Dickinson) software.

GPCR antagonist screen of EPI-X4. Antagonistic activity of EPI-X4 was analyzed by DiscoveRx (Fremont, CA), using their proprietary PathHunter Biosensor Chemokine GPCR, which quantifies GPCR activity using a β-arrestin recruitment-based β-galactosidase enzyme complementation assay. Antagonistic activity was tested against a panel of 18 chemokine receptors. EPI-X4 was used at a concentration of 1 mg/ml and co-incubated with receptor-specific ligand at its EC_{80} concentration. % inhibition rates were calculated relative to basal and EC_{80} activity of relevant ligand alone.

[^{35}S]GTP[S] binding assay. Baculoviruses encoding human CXCR4, rat G protein α_{i2} subunit, and both human G protein β_1 subunit and bovine G protein γ_3 subunit were produced as described (Moepps *et al.*, 1997). [^{35}S]GTP[S] was obtained from Perkin-Elmer (Waltham, MA). CXCL12 was obtained from PeproTech (Rocky Hill). Sf9 cells were grown at 27°C in 59-cm^2

cell-culture dishes in TNM-FH medium (Sigma, T 1032) supplemented with 10% fetal calf serum and 0.5 mg/ml gentamicin. For production of recombinant receptors and heterotrimeric G_{i2}, cells were grown to a density of approximately 60%, incubated for 1 h at 27°C in 2 ml per dish of medium containing the recombinant baculovirus(es). The cells were then supplemented with 9 ml per dish of fresh medium and maintained in this medium for 48 h at 27°C. For the preparation of a crude membrane fractions, cells were pelleted by centrifugation and resuspended in 600 µl per dish of ice-cold lysis buffer containing 20 mM Tris-HCl, pH 7.5, 1 mM EDTA, 3 µM GDP, 2 µg/ml soybean trypsin inhibitor, 1 µM pepstatin, 1 µM leupeptin, 100 µM PMSF, and 1 µg/ml aprotinin. Cells were homogenized by forcing the suspension 6 times through a 0.5 mm x 23 mm needle attached to a disposable syringe. After 30 min on ice, the lysate was centrifuged at 2,450 x g for 45 s to remove unbroken cells and nuclei. A crude membrane fraction was isolated from the resulting supernatant by centrifugation at 26,000 x g for 30 min at 4°C. The pellet was rinsed with 300 µl of lysis buffer, resuspended in 300 µl of fresh lysis buffer, snap-frozen in liquid nitrogen, and stored at -80 °C.

The binding of [^{35}S]GTP to membranes of baculovirus-infected insect cells was assayed as described (Moepps *et al.*, 1997). In brief, membranes (10 µg of protein/sample) were incubated for 60 min at 30°C in a mixture (100 µl) containing 50 mM triethanolamine/HCl, pH 7.4, 1.0 mM EDTA, 5.0 mM $MgCl_2$, 10 µM GDP, and 1.05 nM [^{35}S]GTP[S] (1250 Ci/mmol) in the absence or presence of increasing concentrations of EPI-X4 peptide (0.3–300 µM). The incubation was terminated by rapid filtration through 0.45-µm pore size nitrocellulose membranes (Advanced Microdevices, Ambala Cantonment, India). The membranes were washed, dried, and the retained radioactivity was determined by liquid-scintillation counting.

Cell migration of murine pro-B cells. Murine and human EPI-X4 were provided by U-PEP (Ulm, Germany) and Plerixafor by Calbiochem. BA/F3 cells (murine pro-B cells, kindly provided by Christian Buske, Ulm University) were grown in RPMI 1640 with FCS (10%), L-glutamine, PenStrep (Gibco) and recombinant murine IL-3 (10 ng/ml, R&D Systems). Murine

CXCL12 (100 nM), peptides and Plerixafor in 600 µl medium were added to 24-well plates. Thereafter, transwells with pore sizes of 5.0 µm (Corning® Transwell® polycarbonate membrane cell-culture inserts, Sigma) containing 2.5 x 10^5 BA/F3 cells (150 µl) and the indicated concentrations of peptides or Plerixafor were inserted. As a total cell control ("Input"), 2.5 x 10^5 cells in 150 µl were added directly to 600 µl RPMI 1640 without a transwell. To quantify spontaneous migration, 2.5 x 10^5 cells (150 µl) were added to a transwell in the absence of antagonists, which were then inserted into wells containing medium only (no CXCL12). After 2 h incubation at 37°C, migrated cells were assayed by CellTiter-Glo® Luminescent Cell Viability Assay kit (Promega) as recommended by the manufacturer. The percentage of specifically migrated cells was calculated by i) subtracting values obtained for spontaneous migration (2.8%) from those containing respective chemokines and antagonists, and ii) by dividing these values by those obtained from the total cell input multiplied by 100.

NMR spectroscopy of EPI-X4. For acquisition of NMR spectra, a 1 mM solution of EPI-X4 was prepared in 10 mM Na-phosphate in H_2O/D_2O 10:1, adjusted to a final pH of 7.0 with HCl. TOCSY and NOESY ^{1}H-NMR spectra were recorded at 800 MHz, 600 MHz and 500 MHz on Bruker spectrometers. The spectra acquired in the 800 MHz equipment were used due to their better quality. Spectra were referenced to external TSP, and they were recorded using the States-TPPI method incorporating the watergate 3-9-19 pulse sequence for water suppression (Jeener *et al.*, 1979). In general, 256 equally spaced evolution-time period t_1 values were acquired, averaging 16 transients of 2048 points. Time-domain data matrices were all zero-filled to 4K in both dimensions, thereby yielding a digital resolution of 3.41 Hz/pt. Prior to Fourier transformation, a Lorentz-Gauss window with different parameters was applied to both the t_1 and t_2 dimensions for all the experiments. NOESY spectra (Griesinger *et al.*, 1988) were obtained with mixing times (0.30 s) and TOCSY experiments (Braunschweiler and Ernst, 1983; Rucker and Shaka, 2006) were recorded using 0.060 s DIPSI2 mixing pulses. Both NOESY and TOCSY experiments were performed at 25°C.

NOESY cross-peak assignment and structure calculation of EPI-X4. The ^{1}H chemical shift

dispersion in NMR spectra allowed a straightforward non-ambiguous assignment of all the NH- and CH-alpha resonances, as well as the vast majority of side-chain protons (97.7%), using standard methodology, combining TOCSY and NOESY spectroscopy. The sequential backbone connectivity's were established by following the αCH_i-NH_{i+1} and the NH_i-NH_{i+1} NOEs. Peak lists for the NOESY spectra recorded with a 0.30 s mixing time were generated by interactive peak picking using the XEASY software (Bartels *et al.*, 1995). NOESY cross-peak volumes were determined by the automated peak integration routine, *peakin* implemented in XEASY. The three-dimensional structure of EPI-X4 was determined using the standard protocol of combined automated NOE assignment and structure calculation of the CYANA program (Herrmann *et al.*, 2002; Güntert, 2003, 2004). The 20 best conformers selected showed low CYANA target function values (with mean target function: 0.056). 400 (98.2%) NOESY cross-peaks of the 407 submitted to CYANA were unambiguously assigned by the program. Seven cycles of combined automated NOESY assignment and structure calculations were followed by a final structure calculation. The structure calculation commenced in each cycle from 100 randomized conformers and the standard simulated annealing schedule was used. The 20 conformers with the lowest final CYANA target function values were retained for analysis and passed to the next cycle. Constraint combination was applied in the first two cycles to all NOE distance restraints, spanning at least three residues, in order to minimize structural distortion by erroneous distance restraints. The covalent parameters of Engh and Huber were used (Engh and Huber, 1991). Restraints that involved degenerate groups of protons (e.g. methyls), accidentally degenerated to methylenes, and equivalent aromatic ring protons were expanded into ambiguous distance restraints between all the corresponding pairs of hydrogen atoms. Non-degenerate diastereotopic pairs were periodically swapped for minimal target function values during simulated annealing in cycles 1–7. Weak restraints on φ/ψ torsion angle pairs and on side-chain torsion angles between tetrahedral carbon atoms were temporarily applied during the high-temperature and cooling phases of the simulated annealing schedule in order to favor the permitted regions of the Ramachandran plot and staggered rotamer positions,

respectively. The list of upper distance bonds for the final structural calculation is exclusively comprised of unambiguously assigned upper distance bonds and does not require the possible swapping of diastereotopic pairs.

Structure of EPI-X4. The 20 conformers with the lowest final CYANA target function values bundle tightly (Figure 5A) and, consequently, show a remarkably low RMSD for a peptide of 16 residues (mean global backbone RMSD of 1.73 for the full length polypeptide, 1.26 if residues 1-14 are exclusively considered (Koradi *et al.*, 1996), which allows a significant mean three-dimensional structure of EPI-X4 to be computed, afterwards refined using the AMBER 9 package (Case *et al.*, 2006). As shown in table S3, there are strong long-distance NOEs between the protons of the methyl groups of the N-terminal Leu and those of the ring of Pro9, which reveals the existence of a strong hydrophobic interaction between those two chemical groups. To this interaction the Tyr4 ring is added, the protons of which participate in three medium/large range NOEs with those of the methyl groups of Leu1 (average distance, 4.6 Å), and in six significant and clearly detectable weak NOEs with those of the Pro9 ring (average distance, 5.33 Å). This hydrophobic nucleus causes the backbone of the Leu1-Pro9 stretch to adopt a sort of ring structure (Figure 5B) that orients the lateral chains of Arg3, Lys6, Lys7 plus the N-terminus of Leu1 towards one of its faces, which consequently shows a highly positive charge (Figure 5C). The structural relevance of this ring is clearly underscored by the dramatic decrease in EPI-X4 activity when Leu1 is eliminated (Table S1). The other face of the ring is shielded from the solvent by the rest of EPI-X4, mainly by the stretch Gln10-Pro14 which shows strong hydrophobic interactions with this later face, as shown by the high number of strong NOEs between the protons of the methyl group of the Thr5 lateral chain with those of the ring of Pro14 and side-chain protons of Thr13 and (Table S3). Tyr4 weakly, but clearly, also interacts with Thr13, bridging this last hydrophobic nucleus with the one described above (Figure 5B and Table S3). The clustering of such a high density of charges at one face of EPI-X4 involves a high entropic cost that is obviously exceedingly compensated, as suggested by the strong bundling of conformers resulting from the CYANA calculations by the shielding from the

solvent of the two hydrophobic nuclei described in previous paragraphs. Thus, the EPI-X4 structure is a metastable state in which two forces of opposite directions reciprocally counterpoise, with obvious predominance of one of them. Consequently, this structure constitutes a sort of loaded spring that can abruptly lead to its deep disassembly by small alterations of the elements involved in the balance (vg. elimination of Leu1; Table S1).

Binding model of the natural ligands CXCL12, EPI-X4 and the V3 loop of gp120–to CXCR4. The atomic structure of the cell membrane protein to which EPI-X4 binds, the G protein–coupled chemokine receptor CXCR4, has been recently published, bound to two antagonists (Wu *et al.*, 2010). A representation of the structure of CXCR4 bound to the cyclic peptide CVX15 (PDB entry code: 3OE0) was used to model the binding process of EPI-X4. The electrostatic potential of the CXCR4 surface facing the extracellular space is shown in Figure S3. In this Figure, CVX15 has been detached from the complex to show the deep negatively charged well where the ligands bind. Residues assigned to extracellular loops 2 and 3 in the traditional three-dimensional models of CXCR4 are mainly responsible for the creation of this negatively charged well. This well is probably less defined in the free form than it appears in the figure, as crystallization of CXCR4 seemed unfeasible in the absence of antagonists, and slight differences were observed between the structures of the protein bound to the two different antagonists used for crystallization. Consequently, it seems that there is a certain degree of induced fitting in CXCR4 when the complex forms with its ligands.

Conservation score of EPI-X4 in serum albumins of various species. The following mammalian serum albumin orthologs were included in the sequence analysis:

Species	accession number	amino acids
Homo sapiens (Human)	sp|P02768	25-609
Rattus norvegicus (Rat)	sp|P02770	25-608
Mus musculus (Mouse)	sp|P07724	25-608
Sus scrofa (Pig)	sp|P08835	25-607

1	Oryctolagus cuniculus (Rabbit)	sp|P49065	25-608
2	Bos taurus (Bovine)	sp|P02769	25-607
3	Mesocricetus auratus (Golden hamster)	sp|A6YF56	25-608
4	Canis familiaris (Dog)	sp|P49822	25-608
5	Equus asinus (Donkey)	sp|Q5XLE4	25-607
6	Ovis aries (Sheep)	sp|P14639	25-607
7	Macaca mulatta (Rhesus macaque)	sp|Q28522	17-600
8	Felis catus (Cat)	sp|P49064	25-608
9	Equus caballus (Horse)	sp|P35747	25-607
10	Macaca fascicularis (Cynomolgus monkey)	sp|A2V9Z4	25-608
11	Pongo abelii (Sumatran orangutan)	sp|Q5NVH5	25-609
12	Capra hircus (Goat)	tr|B3VHM9	1-583
13	Meriones unguiculatus (Mongolian gerbil)	sp|O35090	26-609
14	Microtus fortis fortis (Reed vole)	tr|Q5EG49	25-608
15	Sarcophilus harrisii (Tasmanian Devil)	tr|G3WQH5	25-608
16	Cavia porcellus (Guinea pig)	tr|Q6WDN9	25-608
17	Mustela putorius furo (Ferret)	tr|M3YD14	25-608

18

19 Protein sequences were aligned using ClustalW2 (http://www.ebi.ac.uk/Tools/msa/clustalw2/)
20 and residue conservation was determined using the Scorecons Server
21 (http://www.ebi.ac.uk/thornton-srv/databases/cgi-bin/valdar/scorecons_server.pl). The
22 Shannon information theoretical entropy was applied to measure the diversity of amino acids
23 at a specific site. Residues were classified into one of seven types: aliphatic [AVLIMC],
24 aromatic [FWYH], polar [STNQ], positive [KR], negative [DE], special conformations [GP]
25 and gaps (Mirny and Shakhnovich, 1999). Statistical calculations were performed with a two-
26 tailed unpaired Students-t-test using GraphPad Prism Version 5.0. $p < 0.05$ was considered
27 significant.

Serum stability of EPI-X4 and derivatives. Human serum was spiked with 1 mM of EPI-X4 or improved derivatives and incubated at 37°C. Samples were taken every two hours and immediately stored at -20°C. To assess the antiviral activity of the incubated peptide in serum, 10 µl of the samples were added to 5 x 10^3/100 µl TZM-bl cells. Subsequently, the cells were infected with 90 µl HIV-1 NL4-3 resulting in 20-fold dilution of peptide and serum mixtures. Infectivity was measured 2 days after infection using the one-step Tropix Gal-Screen Kit. To assess the effect of protease inhibitors on EPI-X4 degradation, serum was first supplemented with a protease inhibitor cocktail (1X Complete mini (Roche) and 1 mM PMSF (Roche)) before 1 mM EPI-X4 was added.

Effect of CXCL12 and CXCR4 antagonists on actin cytoskeleton. CXCL12-induced cytoskeletal contraction was assessed as previously described (Bonig *et al.*, 2004). Briefly, Jurkat cells preincubated either with medium, EPI-X4 derivatives or Plerixafor (all 545 µM) were stimulated with CXCL12 (100 ng/mL) at 37°C for the indicated time, fixed in 5% formaldehyde (Carl Roth GmbH, Karlsruhe, Germany), and permeabilized with 0.1% saponin (Carl Roth). F-actin was stained with AlexaFluor568-conjugated phalloidin (Molecular Probes, Eugene, OR, USA) followed by flow cytometric analysis of relative staining intensity. Data are expressed as mean±SEM n-fold difference over staining intensity in unstimulated cells for n=4 independent experiments. * indicates $p < 0.05$ compared to CXCL12 alone (no antagonist).

Generation of EPI-X4 in acidified sera from rhesus macaque and mouse. Frozen serum samples from three rhesus macaques (#2324, #2290, #13934) were obtained from the German Primate Centre. Samples were adjusted to pH 4 or left untreated, and were then incubated for 96 h at RT. Thereafter, samples were frozen at -80°C. 35 ml of pooled mouse serum was obtained through the Tierforschungszentrum Ulm, adjusted to pH 4 and incubated for 72 h before samples were frozen. Thereafter, EPI-X4 concentrations were determined by sandwich ELISA using synthetic human or mouse EPI-X4, respectively, as standard.

Detection of EPI-X4 in neutrophil-treated HSA. For isolation of neutrophils, 30 ml of blood was withdrawn and mixed with 10 ml of hydroxyethyl starch (Plasmasteril; Fresenius).

Erythrocytes were sedimented for 45 min at room temperature. The supernatant was centrifuged at 200 × *g* for 20 min. The cell pellet was resuspended in 20 ml of FCS-free RPMI 1640, layered onto 15 ml of Ficoll-Paque (Pharmacia Biotech), and centrifuged at 1,000 × *g* for 15 min at room temperature. The cell pellet was resuspended in RPMI 1640 at a concentration of 1 × 10^7/ml and centrifuged at 200 × g for 20 min. Erythrocytes were lysed by resuspending the pellet in 24 ml double-distilled water for 30 s and subsequent addition of 8 ml of 3.6% NaCl solution. Cells were centrifuged at 500 × *g* for 8 min and resuspended in FCS-free RPMI 1640 medium at a concentration of 2 × 10^7/ml. 5 mg human albumin was resuspended in 250 µl buffer, added to 250 µl of granulocytes and incubated at 37°C. Samples were withdrawn at 0, 1, 5, 10, 20, 60, 120, 180 min, mixed with 0.01 M HCl at a volume ratio of 1:1, and immediately frozen. After thawing, the samples were filtered (0.45 µm) and chromatographed using an analytical reverse phase method, with a Source RPC15 column (250 mm x 10 mm i.d., 12 nm pore size, 15 µm particle size). Separation was performed at a flow rate of 2 ml/min using a linear binary gradient from 100% solvent A (0.1% TFA in water) to 60% solvent B (0.1% TFA in 80% acetonitrile) within 40 min. Fractions of 2 ml were collected. Subsequently, fractions were analyzed by MALDI-MS using a Voyager - DE PRO MALDI-mass spectrometer (Applied Biosystems). The samples were applied to a stainless steel multiple sample tray as an admixture to sinapinic acid using the dried drop technique. Measurements were performed in linear mode. The instrument was equipped with a 1.2-m flight tube and a 337-nm nitrogen laser. Positive ions were accelerated at 30 kV and 64 laser shots were automatically accumulated per sample position. The time-of-flight data were externally calibrated for each sample plate and sample preparation. EPI-X4 was unambiguously identified by sequence analysis using ESI-MSMS (Proteome Factory AG, Berlin).

Generation of EPI-X4 by APCs. Ficoll-isolated peripheral blood mononuclear cells were depleted from non-adherent cells following 24 h of plastic adherence. During three weeks of *in vitro* culture in RPMI1640 (Invitrogen.com) supplemented with 10% fetal calf serum (FCS), 25 mM HEPES and antibiotics, a morphologically homogeneous cell population was enriched

which expressed markers for APC. From 5 ml of heparinized blood, 2 x 10^6 mononuclear cells with a proportion of 10-15% of cells expressing markers for monocytes (CD14+) or dendritic cells (CD11c, CD123/DR) were obtained. Immature APC were amoeboid, floating or loosely adherent and could be readily harvested by gentle agitation. After 21 days, 0.5% of human serum albumin was added. 72 h later, one fraction of the cells were prepared for electron microscopical examination. For this, the classical chemical fixation high-pressure freezing method was applied. Chemical fixation was performed with 2.5% glutar-dialdehyde (grade I, Sigma 5882) for 20 min *in situ*, followed by three washes in PBS and two washes in RPMI1640. Next, fixed cells were treated with 2% osmium tetroxide, dehydrated in a graded series of isopropanol, and block stained with 2% uranyl acetate. Samples were embedded in EPON. Ultra thin sections (80 nm) and cut on a Leica microtome E, stained with 0.2% lead citrate, and imaged using a Jeol 1400 Transmission electron microscope (Jeol.de) at an acceleration of 80kV. In parallel, 2 x 10^4 cells were lysed with 60µl Pharmingen Lysis Buffer (10 mM Tris-HCL (pH 7.5), 10 mM NaH2PO4/NaHPO4, 130 mM NaCl, 1% Triton X-100, 10 mM PPi), for 10 min on ice, centrifuged a 13,000 x g for 30 min. The supernatant containing the plasma membrane vesicles was frozen at -70°C and EPI-X4 was detected by EPI-X4 specific ELISA.

Supplemental references

Bartels, C., Xia, T.H., Billeter, M., Güntert, P., and Wüthrich, K. (1995). The program XEASY for computer-supported NMR spectral analysis of biological macromolecules. J Biomol NMR. *6*, 1–10.

Bonig, H., Priestley, G.V., Nilsson, L.M., Jiang, Y., and Papayannopoulou, T. (2004). PTX-sensitive signals in bone marrow homing of fetal and adult hematopoietic progenitor cells. Blood *104*, 2299–2306.

Braunschweiler, L., and Ernst, R. (1983). Coherence transfer by isotropic mixing: Application to proton correlation spectroscopy. J. Magn. Reson. *53*, 521–528.

Case, D.A., Darden, T., Wong, K., Simmerling, C., and Brozell, S.C. (2006), *AMBER 9*, University of California, San Francisco.

Engh, R.A., and Huber, R. (1991). Accurate bond and angle parameters for X-ray protein structure refinement. Acta Crystallogr D Biol Crystallogr. *47*, 392–400.

Griesinger, C., Otting, G., Wuethrich, K., and Ernst, R.R. (1988). Clean TOCSY for proton spin system identification in macromolecules. J Am Chem Soc. *110*, 7870–7872.

Güntert, P. (2003). Automated NMR protein structure calculation. PROG NUCL MAG RES SP *43*, 105–125.

Güntert, P. (2004). Automated NMR structure calculation with CYANA. Methods Mol Biol. *278*, 353–378.

Hachet-Haas, M., Balabanian, K., Rohmer, F., Pons, F., Franchet, C., Lecat, S., Chow, K.Y., Dagher, R., Gizzi, P., Didier, B., et al. (2008). Small neutralizing molecules to inhibit actions of the chemokine CXCL12. J Biol Chem. *283*, 23189–23199.

Herrmann, T., Güntert, P., and Wüthrich, K. (2002). Protein NMR structure determination with automated NOE assignment using the new software CANDID and the torsion angle dynamics algorithm DYANA. J Mol Biol. *319*, 209–227.

Jeener, J., Meier, B.H., Bachmann, P., and Ernst, R.R. (1979). Investigation of exchange processes by two-dimensional NMR spectroscopy. J. Chem. Phys. *71*, 4546.

Koradi, R., Billeter, M., and Wüthrich, K. (1996). MOLMOL: a program for display and analysis of macromolecular structures. J Mol Graph. *14*, 51-5, 29-32.

Mirny, L.A., and Shakhnovich, E.I. (1999). Universally conserved positions in protein folds: reading evolutionary signals about stability, folding kinetics and function. J Mol Biol. *291*, 177–196.

Moepps, B., Frodl, R., Rodewald, H.R., Baggiolini, M., and Gierschik, P. (1997). Two murine homologues of the human chemokine receptor CXCR4 mediating stromal cell-derived factor 1alpha activation of Gi2 are differentially expressed in vivo. Eur J Immunol. *27*, 2102–2112.

O'Brien, P.J., Irwin, W., Diaz, D., Howard-Cofield, E., Krejsa, C.M., Slaughter, M.R., Gao, B., Kaludercic, N., Angeline, A., Bernardi, P., et al. (2006). High concordance of drug-induced human hepatotoxicity with in vitro cytotoxicity measured in a novel cell-based model using high content screening. Arch Toxicol. *80*, 580–604.

Rucker, S.P., and Shaka, A.J. (2006). Broadband homonuclear cross polarization in 2D N.M.R. using DIPSI-2. Mol. Phys. *68*, 509–517.

Wu, B., Chien, E., Mol, C.D., Fenalti, G., Liu, W., Katritch, V., Abagyan, R., Brooun, A., Wells, P., Bi, F.C., et al. (2010). Structures of the CXCR4 chemokine GPCR with small-molecule and cyclic peptide antagonists. Science *330*, 1066–1071.